Sequential and compartmentalized action of Rabs, SNAREs, and MAL in the apical delivery of fusiform vesicles in urothelial umbrella cells

Bret Wankel[a], Jiangyong Ouyang[a], Xuemei Guo[a], Krassimira Hadjiolova[a], Jeremy Miller[a], Yi Liao[a], Daniel Kai Long Tham[a], Rok Romih[b], Leonardo R. Andrade[c], Iwona Gumper[a], Jean-Pierre Simon[a], Rakhee Sachdeva[a], Tanya Tolmachova[d], Miguel C. Seabra[d], Mitsunori Fukuda[e], Nicole Schaeren-Wiemers[f], WanJin Hong[g], David D. Sabatini[a], Xue-Ru Wu[h], Xiangpeng Kong[i], Gert Kreibich[a], Michael J. Rindler[a,*], and Tung-Tien Sun[a,h,i,j,*]

[a]Department of Cell Biology, [h]Department of Urology, [i]Department of Biochemistry and Molecular Pharmacology, and [j]Department of Dermatology, New York University School of Medicine, New York, NY10016; [b]Institute of Cell Biology, Faculty of Medicine, University of Ljubljana, SI-1000 Ljubljana, Slovenia; [c]Institute of Biomedical Sciences, Federal University of Rio de Janeiro, Rio de Janeiro 21941-902, Brazil; [d]Molecular and Cellular Medicine, Imperial College, London SW7 2AZ, United Kingdom; [e]Department of Developmental Biology and Neurosciences, Graduate School of Life Sciences, Tohoku University, Sendai 980-8578, Japan; [f]Neurobiology Laboratory, Department of Biomedicine, University Hospital Basel, University of Basel, CH-4031 Basel, Switzerland; [g]Cancer and Developmental Cell Biology Division, Institute of Molecular and Cell Biology, A*STAR, Biopolis, Singapore 138673

ABSTRACT **Uroplakins (UPs) are major differentiation products of urothelial umbrella cells and play important roles in forming the permeability barrier and in the expansion/stabilization of the apical membrane. Further, UPIa serves as a uropathogenic *Escherichia coli* receptor. Although it is understood that UPs are delivered to the apical membrane via fusiform vesicles (FVs), the mechanisms that regulate this exocytic pathway remain poorly understood. Immunomicroscopy of normal and mutant mouse urothelia show that the UP-delivering FVs contained Rab8/11 and Rab27b/Slac2-a, which mediate apical transport along actin filaments. Subsequently a Rab27b/Slp2-a complex mediated FV–membrane anchorage before SNARE-mediated and MAL-facilitated apical fusion. We also show that keratin 20 (K20), which forms a chicken-wire network ~200 nm below the apical membrane and has hole sizes allowing FV passage, defines a subapical compartment containing FVs primed and strategically located for fusion. Finally, we show that Rab8/11 and Rab27b function in the same pathway, Rab27b knockout leads to uroplakin and Slp2-a destabilization, and Rab27b works upstream from MAL. These data support a unifying model in which UP cargoes are targeted for apical insertion via sequential interactions with Rabs and their effectors, SNAREs and MAL, and in which K20 plays a key role in regulating vesicular trafficking.**

Monitoring Editor
Keith E. Mostov
University of California, San Francisco

Received: Apr 23, 2015
Revised: Mar 15, 2016
Accepted: Mar 17, 2016

This article was published online ahead of print in MBoC in Press (http://www.molbiolcell.org/cgi/doi/10.1091/mbc.E15-04-0230) on March 23, 2016.

*Address correspondence to: Tung-Tien Sun (sunt01@nyumc.org), Michael J. Rindler (Michael.Rindler@nyumc.org).

Abbreviations used: DKO, double knockout; EM, electron microscopy; FV, fusiform vesicle; IF, immunofluorescence; K20, keratin 20; KO, knockout; MAL, myelin-and-lymphocyte protein; MDCK, Madin–Darby canine kidney; SNARE, soluble *N*-ethylmaleimide–sensitive factor attachment protein receptor; Wt, wild type.

INTRODUCTION

The targeting of proteins to a particular membrane subdomain, such as the apical surface of epithelial cells, is a vitally important cellular function. The terminally differentiated superficial umbrella cells of the multilayered bladder urothelium provide an excellent model system for the study of apical targeting because they synthesize a large amount of apically targeted uroplakins, a group of integral membrane proteins that form two-dimensional (2D) crystalline "plaques" that cover almost the entire urothelial apical surface (Wu *et al*., 1990, 1994, 2009; Lin *et al*., 1994; Yu *et al*., 1994; Sun *et al*., 2013).

Supplemental Material can be found at:
http://www.molbiolcell.org/content/suppl/2016/03/21/mbc.E15-04-0230v1.DC1.html

There are four major uroplakins (UPs): UPIa and UPIb belong to the tetraspanin family and have four transmembrane domains (TMDs; Wu *et al.*, 1990; Yu *et al.*, 1990, 1994), whereas UPII and IIIa have a single TMD and share a juxtamembrane stretch of ~12 amino acid residues (Wu *et al.*, 1990; Wu and Sun, 1993; Lin *et al.*, 1994). Although cotransfection studies demonstrated that these can exist independently as Ia/II and Ib/IIIa heterodimers, they pair to form Ia/II-Ib/IIIa tetramers, which then hexamerize to form 16-nm particles upon exit from the endoplasmic reticulum (Tu *et al.*, 2002; Hu *et al.*, 2005, 2008). These particles are hexagonally packed to form urothelial plaques that are flattened and rigid looking (Kachar *et al.*, 1999). Two of these plaques, interconnected by a flexible "hinge," form a fusiform vesicle (FV), which deliver the two plaques to the apical membrane (Kachar *et al.*, 1999; Liang *et al.*, 1999; Hudoklin *et al.*, 2012). The structure of the uroplakin plaques has been studied by negative staining, quick-freeze deep-etch, and cryo–electron microscopy (EM), which yielded a uroplakin structural model at 6-Å resolution (Walz *et al.*, 1995; Min *et al.*, 2003, 2006). Gene ablation and physiological studies showed that uroplakins have important biological functions, including the formation of a highly effective urothelial permeability barrier (Hu *et al.*, 2000, 2002; Kong *et al.*, 2004), the expansion and stabilization of the apical surface (Hu *et al.*, 2000; Kong *et al.*, 2004), and the reversible adjustment of the umbrella cell apical surface area during the micturition cycle (Lewis and de Moura, 1982; Truschel *et al.*, 2002; Wang *et al.*, 2005; Yu *et al.*, 2009). In addition, uroplakin Ia serves as a receptor for type 1 fimbriated uropathogenic *Escherichia coli* (Wu *et al.*, 1996; Zhou *et al.*, 2001; Liu *et al.*, 2015).

Regulated exocytosis of the FV is coordinated by Rab GTPases, a family of proteins that can direct vesicular traffic (Agola *et al.*, 2011; Hutagalung and Novick, 2011). We showed previously that Rab27b but not its closely related Rab27a is highly enriched in urothelial umbrella cells, where it localizes to FVs (Chen *et al.*, 2003). In addition, Khandelwal *et al.* (2008, 2013) reported that Rab11a is involved in the initial transport of vesicles from the *trans*-Golgi network (TGN), whereas Rab8a and myosin Vb are responsible for subsequent trafficking of FVs to the cell surface. Beyond this, however, the precise roles of Rab27b and its relationship with the Rabs11/8 pathway in FV trafficking remain unclear.

Myelin-and-lymphocyte protein (MAL, or VIP17) is another major component in FV exocytosis and is associated with the FV hinge (Zhou *et al.*, 2012). Conflicting data exist regarding the role of MAL in epithelial protein trafficking. Some investigators suggested that MAL functions in the sorting of apical membrane proteins in the TGN (Cheong *et al.*, 1999; Puertollano and Alonso, 1999; Puertollano *et al.*, 1999). However, we showed that in Madin–Darby canine kidney (MDCK) cells, via knockdown experiments, and in mutant mouse urothelia (MAL knockout and overexpression), MAL plays no role in apical targeting. Instead, it facilitates the apical fusion of the uroplakin vesicles (Zhou *et al.*, 2012). Thus the precise roles of MAL in FV trafficking remain to be established.

It has also been reported that soluble *N*-ethylmaleimide–sensitive factor attachment protein receptor (SNARE) proteins (Jahn and Scheller, 2006) are present in FVs and the apical surface in urothelial umbrella cells in rats, suggesting that these proteins may play a role in mediating FV fusion (Born *et al.*, 2003). However, which SNAREs are present and what their role is in the urothelium are poorly understood.

In this work, we study uroplakin exocytosis by colocalizing uroplakins with a number of trafficking molecules in mouse urothelial umbrella cells. In addition, we examine the phenotypes of several genetically modified mice, including Rab27b-, VAMP8-, and MAL-knockout animals, as well as mice carrying inactivating mutations of the Rab27b effector, Slac2-a. Our results show that uroplakin vesicles are targeted to the apical membrane via sequential interactions with Rab11, Rab8, and Rab27b, and their effectors, culminating in a final step of SNARE-mediated and MAL-facilitated apical fusion. We also demonstrate that a dense network of keratin 20 (K20) defines a subapical compartment containing uroplakin vesicles that are primed for apical fusion. On the basis of these data, we propose a unifying model in which UP cargoes are targeted for apical insertion via sequential interactions with Rabs and their effectors, SNAREs and MAL, and in which K20 plays a key role in regulating vesicular trafficking

RESULTS

Rab27b-containing vesicles reside subapically above a K20 keratin-rich zone

We showed previously that Rab27b localized mainly near the apical membrane of umbrella cells (Chen *et al.*, 2003). Given that keratin K20 forms a subapical band in this region (Moll *et al.*, 1990; Veranic and Jezernik, 2002), we investigated the relationships between K20, UPIIIa, and Rab27b by immunostaining (Figure 1). Our data confirmed those of Veranic and Jezernik (2002), who showed that K20 forms a subapical, chicken wire–like lattice that partially excludes uroplakins (Figure 1A) and had holes large enough to permit FV traffic, as shown by immunostaining of tangential sections (Figure 1B) and whole-mount preparations (Figure 1C). Rab27b was localized above the K20 zone (Figure 1D) in close association with the apical membrane (Figure 1E3), as observed after double staining of Rab27b and K20.

Rab27b deficiency reduces the uroplakin content of umbrella cells

To understand the functional significance of Rab27b, we compared wild-type (Wt) and Rab27b-null mouse urothelium (Tolmachova *et al.*, 2007). Immunofluorescence (IF) microscopy revealed that in normal urothelium, both Rab27b and uroplakin UPIIIa were enriched in upper cell layers (Figure 2A; Chen *et al.*, 2003) and that in Rab27b-knockout mice (Figure 2B1), there was a decrease in uroplakin staining in umbrella cells (Figure 2B2; cf. Figure 2A2). This decrease was measured by quantification of the UPIIIa staining intensity in umbrella cells outlined by pericellular keratin 8 (K8) staining (Figure 2, C and D) and corroborated by transmission EM (TEM) results showing diminished FVs (Figure 2, F and G). The decrease in UP was Rab27b specific. A mouse strain (*ashen*) carrying an inactivating mutation in Rab27a (Barral *et al.*, 2002; Tolmachova *et al.*, 2007), which is closely related but not expressed in urothelium (Chen *et al.*, 2003), had no differences in umbrella cell ultrastructure (Figure 2H) or uroplakin staining intensity (unpublished data). In addition, Rab27b knockout did not induce compensatory Rab27a expression in urothelium (Figure 2E). These data established that deficiency in Rab27b led to a reduced uroplakin level in umbrella cells.

Rab11 and Rab8 are located primarily on uroplakin vesicles below the K20 zone

As noted earlier, Khandelwal *et al.* (2008, 2013) reported that Rab11 and subsequently Rab8 mediate stretch-induced apical uroplakin delivery. They also suggested that Rab27b functions in a separate constitutive exocytic pathway (Khandelwal *et al.*, 2013). To determine the sites of action of these Rabs, we localized all three of them, as well as several of their effector proteins, in conjunction with UPIIIa and K20 (Figure 3). We found that most of the Rab11 was located below the K20 zone (Figure 3A) and Rab27b (Figure 3B). Of interest, some of the Rab11 overlapped with Rab27b (Figure 3B) and UPIIIa (Figure 3C), and in these cases, we could show by triple staining the

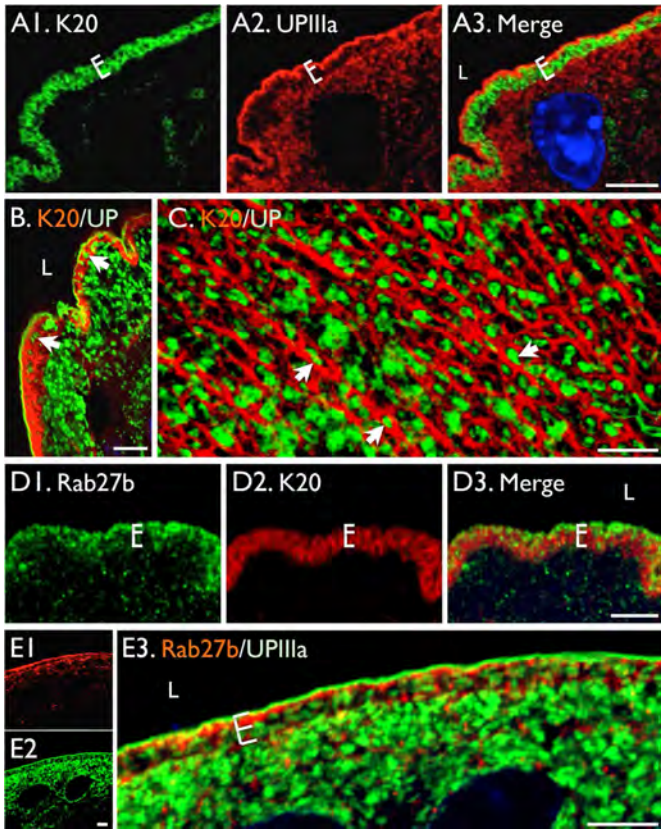

FIGURE 1: A subapical keratin K20 band defines a compartment containing most of the Rab27b-associated FVs in umbrella cells. Paraffin sections of mouse bladder or a whole-mount (C) of the urothelium were immunostained for confocal microscopy. (A1–A3) Double staining of K20 (A1) and UPIIIa (A2), showing a subapical, dense keratin K20 band (brackets) and the partial exclusion of uroplakins from this band; a merged image is shown in A3. L, lumen of the bladder. Note that the K20 band was 200 ± 100 nm (SD) below the apical surface and was 1.75 ± 0.45 µm thick. (B, C) Double staining of keratin 20 (red) and uroplakin (green) in a tangential section (B), showing holes in the K20 (arrows), and in a mouse bladder whole mount (C), showing an extensive chicken wire–like K20 network with hole sizes slightly larger than the FVs (0.6–0.8 µm in diameter). (D1–D3) Double staining of Rab27b (D1) and K20 (D2), showing that Rab27b is mostly located above the K20 zone (brackets). (E1–E3) Double staining of Rab27b (red) and UPIIIa (green), showing the close association of Rab27b-containing vesicles with the apical membrane. Bars, 5 µm.

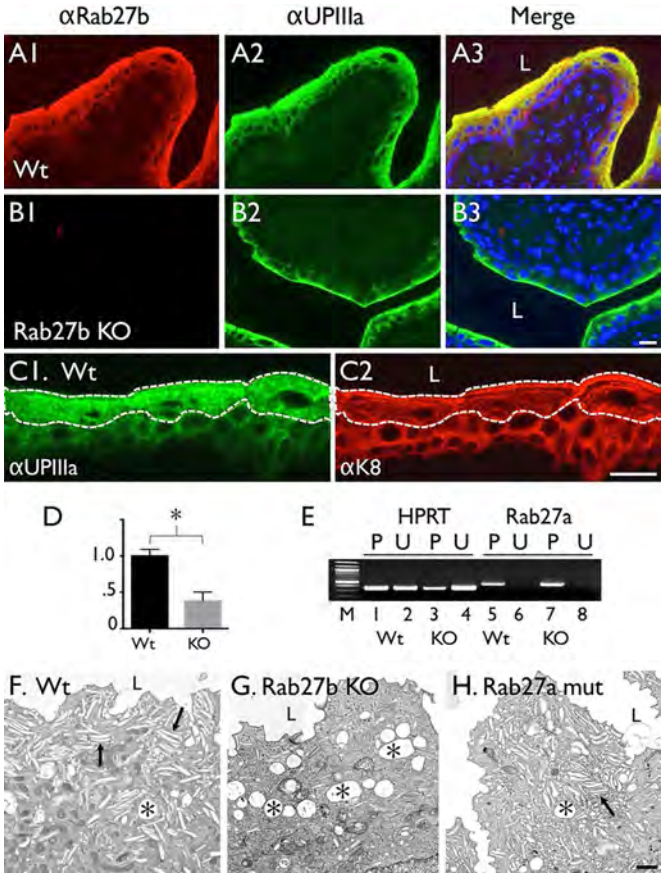

FIGURE 2: Rab27b-null mouse urothelium has reduced uroplakin level. (A, B) Paraffin sections of Wt (A) and Rab27b-KO (B) mice were double stained for IF microscopy using antibodies to Rab27b (A1, B1) and UPIIIa (A2, B2). All images had the same exposure time. Note decreased UP staining in the Rab27b-KO urothelium (B2 vs. A2). (C1, C2) Double staining of a section of Wt urothelium using antibodies to UPIIIa (C1) and keratin 8 (K8; C2), showing the umbrella cells (dashed lines). (D) Quantification of IF staining intensities in the urothelial umbrella cells of Wt and Rab27b KO urothelia. The intensity of UPIIIa (mean ± SEM) was significantly lower than that of Wt (*$p < 0.0001$; $n = 6$; two images from each section from three independent experiments; arbitrary units, Wt = 1.0). (E) RT-PCR detection of hypoxanthine phosphoribosyltransferase 1 (HPRT; loading controls; lanes 1–4) and Rab27a (lanes 5–8) of mouse pancreas (P; odd lanes) or bladder urothelium (U; even lanes) from Wt (lanes 1, 2, 5, and 6) and Rab27b KO mice (lanes 3, 4, 7, and 8). M, molecular weight markers. Note that Rab27b KO did not induce the expression of Rab27a, an isoform of Rab27b. (F–H) TEM of urothelia from Wt (F), Rab27b-null (G), and Rab27a mutation mice (H; *ashen* mice). Note that a representative image of the Rab27b KO urothelium (G) has fewer fusiform vesicles (arrows) and prominent multivesicular bodies (*), whereas Rab27a mutant urothelium (H) has normal morphology. Bars, 20 µm (A–C), 1 µm (F–H).

existence of UP vesicles containing both Rab11 (Figure 3D1) and Rab27b (Figure 3D2). Similarly, Rab8 was mostly located below the K20 (Figure 4A) and Rab27b zones (Figure 4B). In some areas, Rab8 could be seen to colocalize with UPIIIa (Figure 4C) and the Rab27b effector myosin Va (Figure 4D) in an actin-containing subapical zone (Figure 4E). We studied myosin Va here, instead of Vb (Khandelwal *et al.*, 2013), because it specifically interacts with the Rab27b/Slac2-a complex (Fukuda, 2013). Like myosin Vb, myosin Va also associates with both Rab11a and Rab8a (Roland *et al.*, 2009; Sun *et al.*, 2014). Together these results suggest that Rab11 and Rab8 functioned mainly below the K20 zone (Figures 3 and 4) and upstream from the apically enriched Rab27b (Figure 1).

Rab27b-associated proteins in urothelial umbrella cells

We determined which Rab27b-binding partners were present in mouse urothelial extracts by reverse transcription (RT)-PCR (Figure 5A) and immunoblotting (Figure 5B) and identified Slp1, Slp2-a, Slp4-a, Slp5-a, and Slac2-a. We next screened our antibodies and found that those against Slp2-a and Slp4-a worked well in immunoprecipitation assays. They pulled down Slp2-a/Rab27b and Slp4-a/Rab27b complexes, respectively (Figure 5C). Of interest, neither of these two antibodies pulled down an Slp2-a/Slp4-a/Rab27b tertiary complex (Figure 5C), indicating that Rab27b bound to Slp2-a or Slp4-a in a mutually exclusive manner. This is consistent with the fact that Slp2-a and Slp4-a share a Rab27b-binding site (the SHD

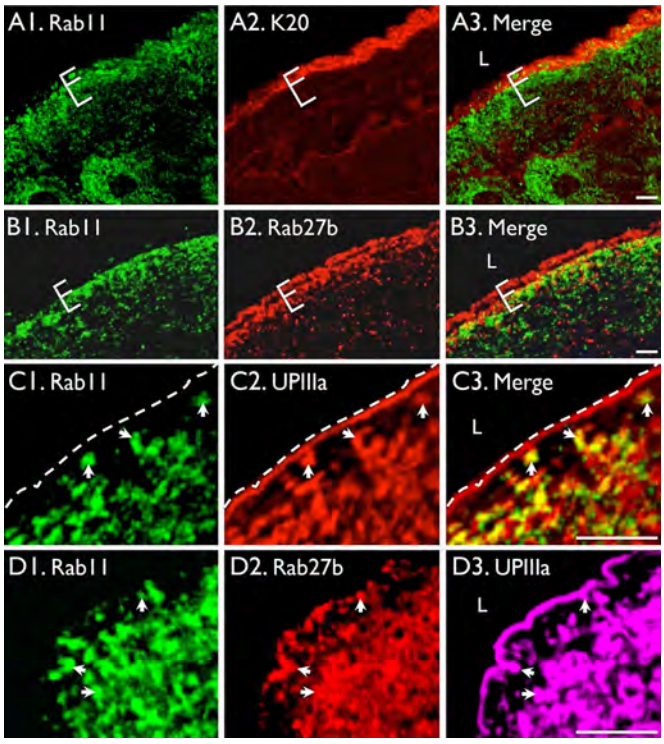

FIGURE 3: Rab11 was largely located below the K20 network. Paraffin sections of mouse bladder were double (A–C) or triple stained (D) for confocal microscopy using antibodies to (A) Rab11 (A1) and K20 (A2); (B) Rab11 (B1) and Rab27b (B2); (C) Rab11 (C1) and UPIIIa (C2); and (D, triple staining) Rab11 (D1), Rab27b (D2), and UPIIIa (D3). Note that in A, most of the Rab11 was below the K20 band; in B, some of the Rab11 overlapped with Rab27b slightly below the K20 zone; in C, Rab11 was colocalized well (arrows) with uroplakin IIIa; and in D, some uroplakin (UPIIIa-positive) vesicles contained both Rab11 and Rab27b (arrows). Bars, 5 μm.

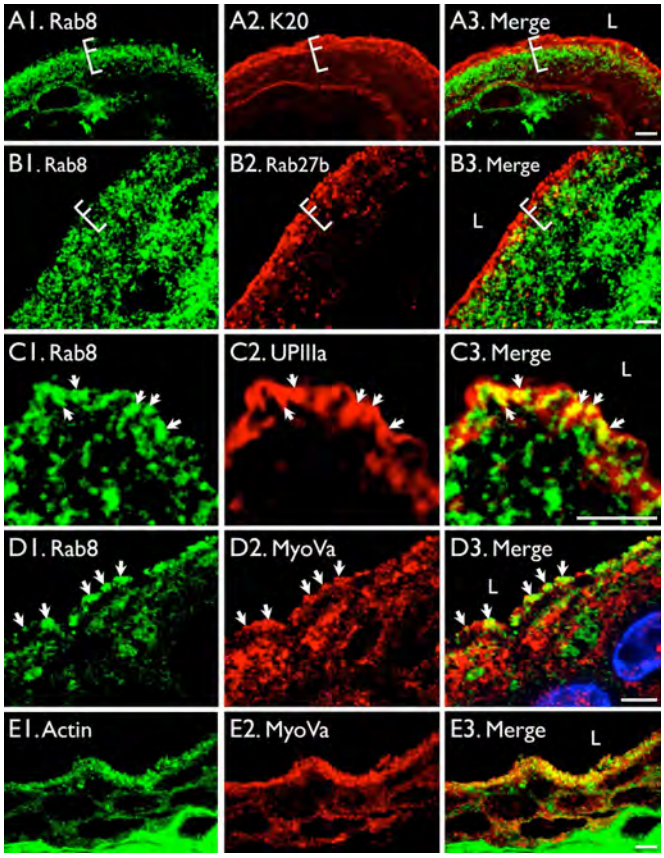

FIGURE 4: Rab8 was largely located below the K20 network. Paraffin (A, B, and D) or frozen (C, E) sections of mouse bladder sections were double stained for confocal microscopy using antibodies to (A) Rab8 (A1) and K20 (A2); (B) Rab8 (B1) and Rab27b (B2); (C) Rab8 (C1) and uroplakin IIIa (C2); (D) Rab8 (D1) and myosin Va (D2); and (E) actin (E1) and myosin Va (E2). Note that Rab8 is largely located (brackets) below the K20 network (A) and the Rab27b zone (B), some of the Rab8 is colocalized (arrows) with UPIIIa (C) and myosin Va (D), and actin (E1) and myosin Va (E2) are present in the subapical zone. Bars, 5 μm.

domain; Fukuda, 2006). Finally, in extracts of Rab27b-knockout mice, we found reduced urothelial levels of some Rab27b-binding partners, including Slp2-a and Slp-5 (Figure 5D; for IF staining of Slp2-a, also see Figure 8E).

Formation of the Rab27b/Slac2-a/myosin Va/actin complex on uroplakin vesicles

In melanocytes and other cell types, Slac2-a forms a tripartite complex with Rab27 and myosin Va to mediate vesicle transport along actin filaments to the cell periphery (Wu *et al.*, 2002). We found in umbrella cells that Slac2-a was highly concentrated in the K20 zone (Figure 6, A1 and B1) containing uroplakin-positive FVs (Figure 6B2). Some Slac2-a staining extended above the K20 zone, where it overlapped with Rab27b (Figure 6C) and myosin Va (Figure 6D).

Slac2-a has an actin-binding domain separate from its myosin Va-binding site (Fukuda and Kuroda, 2002). Indeed, subapical staining for Slac2-a overlapped with that of actin (Figure 6E), although, as previously reported, the actin staining was relatively weak in this region (Romih *et al.*, 1999; Khandelwal *et al.*, 2013). To understand the functional importance of Slac2-a, we studied the effects of its inactivation in the umbrella cells of *leaden* mice, which carry a Slac2-a–inactivating mutation (Fukuda, 2002; Nagashima *et al.*, 2002). The results showed that Slac2-a inactivation led to an umbrella cell phenotype similar to that observed in the Rab27b-knockout mice, including a reduced cell height (between arrows in Figure 7, A–C; quantified in D, top), reduced UP staining (quantified in Figure 7D, bottom), and a reduced number of fusiform vesicles by TEM (Figures 2G and 7E).

Formation of the Rab27b/Slp2-a complex on uroplakin vesicles

Slp2-a, another Rab27b-associated protein that was expressed in urothelium (Figure 5B), was highly enriched, like Rab27b, in the subapical compartment above the K20 zone (Figure 8, A and B). In triple-staining experiments, Slp2-a colocalized well with Rab27b (Figure 8C2) and uroplakin IIIa (Figure 8C3). Moreover, we found that Rab27b knockout selectively and drastically reduced Slp2-a staining of the umbrella cells (compare Figure 8, D1 vs. E1, and D3 vs. E3). Immuno-EM studies showed that Slp2-a was associated with fusiform vesicles near the apical surface of Wt umbrella cells and was absent in the Rab27b-null mice (Figure 8, F and G). These results indicate that in urothelial umbrella cells, Slp2-a is associated with, and stabilized by, Rab27b.

Identification of the urothelial SNAREs and effects of VAMP8 knockout

To understand the possible roles of SNARE proteins in uroplakin delivery, we identified several SNAREs in mouse urothelium by

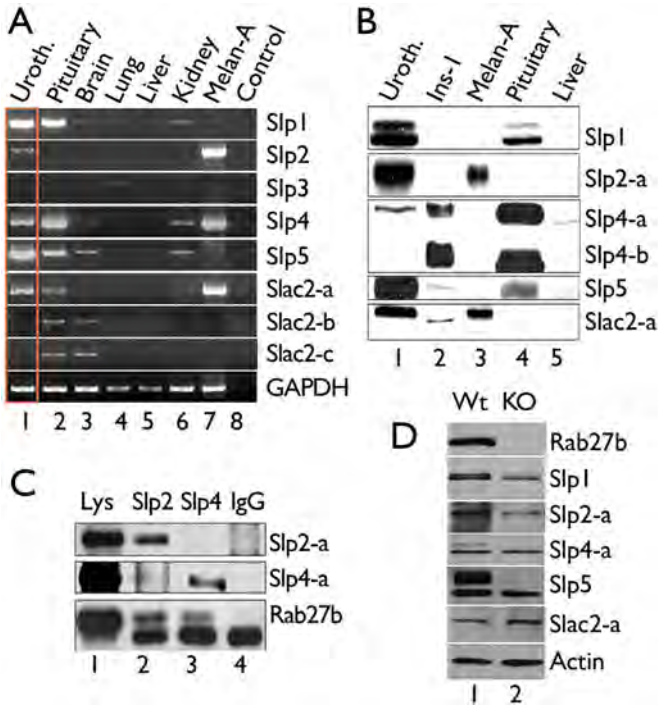

FIGURE 5: Identification of the mouse urothelial Rab27b-associated proteins and their interactions with Rab27b. (A) Detection by RT-PCR of the urothelial mRNAs encoding Rab27b-binding proteins in RNA preparations from (lane 1) mouse urothelium, (2) pituitary, (3) brain, (4) lung, (5) liver, (6) kidney, (7) Melan-A cells, and (8) a no-template control. (B) Immunoblot detection of the Rab27b-interacting proteins in the total proteins of (lane 1) mouse urothelium, (2) an insulin-secreting cell line (Ins-1), (3) Melan-A cells, (4) mouse pituitary, and (5) liver. (C) Coimmunoprecipitation of Rab27b with Slp2-a and Slp4-a. Mouse urothelial proteins solubilized with 0.25% Triton X-100 were resolved by SDS–PAGE either (lane 1) directly or after immunoprecipitation with antibodies to (2) Slp2-a, (3) Slp4-a, or (4) control immunoglobulin G (IgG). The resolved proteins were then immunoblotted using antibodies to Slp2-a (top), Slp4-a (middle), or Rab27b (bottom). The band below Rab27b represents the IgG light chain. Note that Rab27b coimmunoprecipitated with both Slp2-a and Slp4-a in a mutually exclusive manner. (D) Effects of Rab27b KO on the levels of its associated proteins, as assessed by immunoblotting of urothelial extracts; actin was used as a loading control.

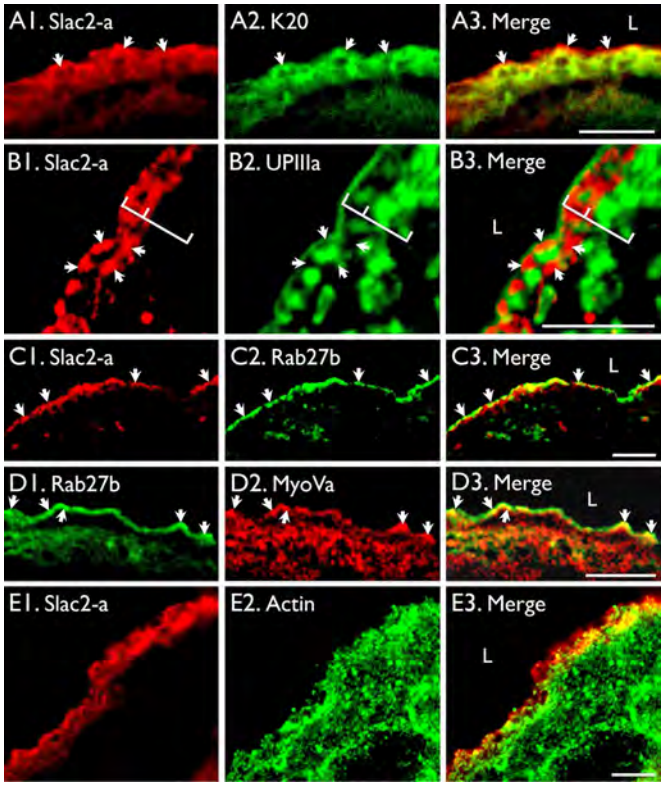

FIGURE 6: Immunolocalization of Slac2-a and its interacting proteins. Paraffin (A–D) or frozen (E) sections of mouse bladder were double stained for confocal microscopy using antibodies to (A) Slac2-a (A1) and K20 (A2); (B) Slac2-a (B1) and UPIIIa (B2); (C) Slac2-a (C1) and Rab27b (C2); (D) Rab27b (D1) and myosin Va (D2); and (E) Slac2-a (E1) and actin (E2). Note in A the high concentration of Slac2-a in the K20 zone and slightly above it; in B, the strong Slac2-a staining (arrows) surrounding the UPIIIa-containing FV; in C, the colocalization of Slac2-a with Rab27b (arrows), and in D, with myosin Va (arrows); and in E, the presence of Slac2-a and actin near the K20 zone (also see Figure 4E1). Bars, 5 µm.

immunoblotting (Figure 9), including target (t)-SNAREs (syntaxins 2, 3, and 11, as well as SNAP23) and vesicle (v)-SNAREs (VAMPs 7 and 8 and Vti1b). Although it had been reported that rat bladder urothelium expressed syntaxin 1 and VAMP2 (Born *et al.*, 2003), we could not detect them in either mouse (Figure 9) or rat urothelium (unpublished data). SNAP23 (Figure 10A) and syntaxin 2 (Figure 10B) appeared to be associated with the apical surface, whereas syntaxin 11 was mostly on cytoplasmic vesicles (Figure 10C). VAMP8 was partially colocalized with the UPIIIa-labeled FVs (Figure 10D) and MAL (Figure 10E), which, we showed earlier, is associated with the hinge region of FVs (Zhou *et al.*, 2012). By immuno-EM, we confirmed that VAMP8 was associated with FVs (Figure 11F). To understand the functional importance of VAMP8, we examined the effects of knocking out its gene in mice (Wang *et al.*, 2004, 2007; Figure 11, A and B). VAMP8 knockout led to a dramatic change in urothelial morphology, that is, the normally three- or four-layered "stratified squamous" urothelium was replaced by a much thicker, stratified columnar epithelium with much smaller superficial cells (15–25 instead of 60–90 µm in diameter; Figure 11, C–E, G and H). TEM images showed that the superficial cells had more multivesicular bodies (Figure 11H).

Using high-resolution scanning EM, we confirmed that the VAMP8-null superficial cells were much smaller (15–25 µm; Figure 11K) than normal and observed that their apical surfaces lacked urothelial plaques (Figure 11L). These phenotypes were similar to those of uroplakin knockouts (KOs; Hu *et al.*, 2000; Kong *et al.*, 2004) but distinct from those of the Rab27b KO, which had a relatively normal apical membrane covered with urothelial plaques (Figure 11M; see *Discussion*). Of interest, we found many invaginations on the apical surface of the normal mouse umbrella cells that were in the size range of uroplakin plaques (Figure 11J, arrows). These invaginations were present in the Rab27b KO but absent in the VAMP8 KO (see *Discussion*).

Phenotype of the urothelium in MAL-Rab27b double-knockout mice

As noted earlier, MAL is associated with the hinge areas of the FVs (Zhou *et al.*, 2012). This association could be seen even more clearly when viewed in tangential tissue sections (Figure 12A) and in whole mounts in the form of small dots of MAL surrounding the uroplakin vesicles (Figure 12B). Furthermore, we found that MAL was enriched

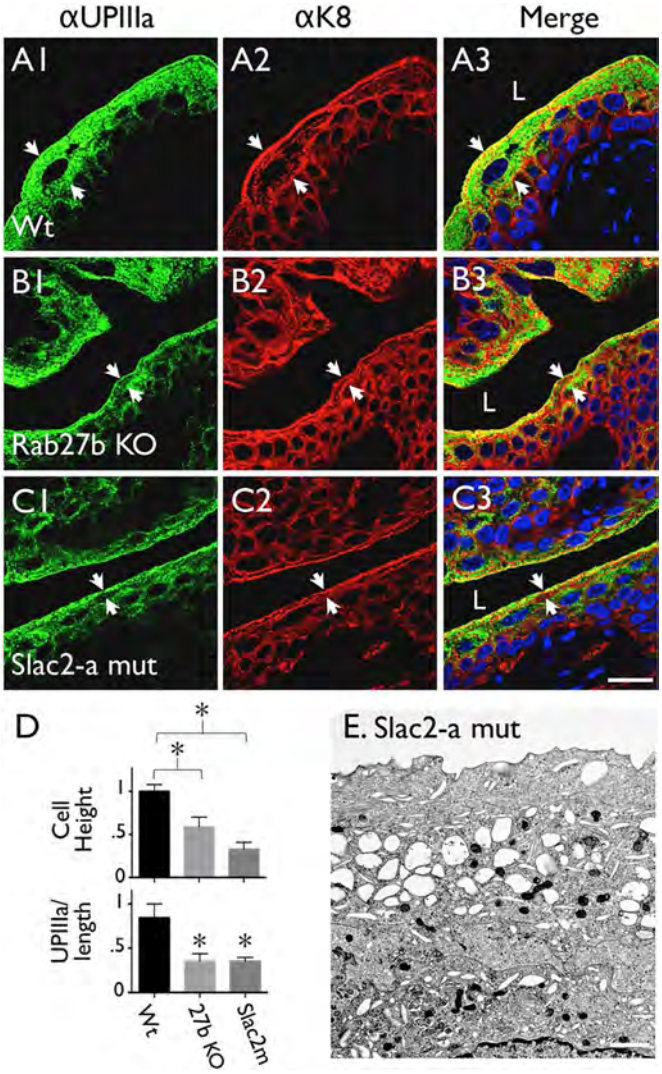

FIGURE 7: UPIIIa levels were reduced in umbrella cells of Rab27b-null and Slac2-a mutant mice. Paraffin sections of Wt (A), Rab27b-KO (B), and Slac2-inactivating mutant (Slac2*; C) bladders were double stained for confocal microscopy using antibodies to uroplakin IIIa (A1, B1, and C1) and K8 (A2, B2, and C2). Note that the urothelia of both Rab27b-KO (B) and Slac2* (C) had thinner umbrella cells (with dense pericellular K8 staining; between arrows) and weaker UPIIIa IF staining than the Wt (A). Bar, 10 μm. (D) Quantification (as described in Figure 2C) showed that a decrease in the integrated UPIIIa IF staining intensity in the umbrella cells of the two mutant mice was statistically significant (*$p < 0.0001$; Wt and Rab27b data are the same as in Figure 2D; five images from two separate sections). Cell height was also markedly reduced (*$p < 0.01$; same images as top). (E) Representative TEM image of the Slac2-a mutant mouse urothelium, showing decreased FVs and increased multivesicular bodies, similar to the Rab27b-null mice (Figure 1, F and G). Bar, 1 μm.

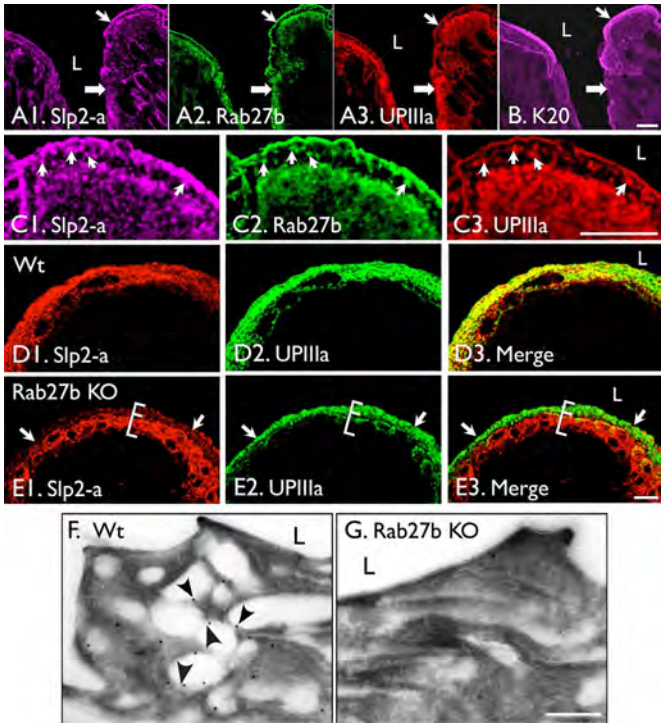

FIGURE 8: Immunolocalization of Slp2-a and its interacting proteins. Paraffin sections from Wt or Rab27b-KO (E) bladders were double- or triple-immunostained for confocal microscopy using antibodies to (A, B) Slp2-a (A1; triple staining of a single section), Rab27b (A2), UPIIIa (A3), or K20 (B; staining of a neighboring section). Note the enrichment of all four antigens in the subapical zone (thin arrow) and the enhanced subapical UP accumulation in areas with less K20 staining (thick arrow). (C) Triple staining: Slp2-a (C1), Rab27b (C2), and UPIIIa (C3). Note the colocalization of the three antigens on the apical membrane, with some uroplakin vesicles just underneath it, as well as in the K20 network (arrows). (D, E) Immunostaining of Slp2-a (D1, E1) and UPIIIa (D2, E2). Note, in E, the disappearance of Slp2-a (arrows) in the Rab27b-KO umbrella cells (brackets). Bars, 10 μm. (F, G). TEM localization of Slp2-a (arrowheads) in the FVs of Wt (F) but not Rab27b-KO urothelia (G), consistent with the IF results. Bars, 0.5 μm.

in the subapical zone (Figure 12C), where it colocalized well with Rab27b (Figure 12D). To critically test our earlier suggestion that MAL is involved in FV fusion with the apical membrane (Zhou *et al.*, 2012), we compared the phenotypes of mouse urothelia that are null in Rab27b, MAL, or both (double knockout [DKO]; Figure 13). Control experiments confirmed that the urothelia of the DKO mice were devoid of both Rab27b and MAL, as assessed by RT-PCR (Figure 13A), immunoblotting (Figure 13B), and IF staining (Figure 13F, 1 and 2). We found that, as was true in the Rab27b KO, the DKO urothelium had a reduced uroplakin IF staining (Figure 13, F3 vs. C3; quantified in G), suggesting that Rab27b acted upstream from MAL in the UP exocytic pathway (see *Discussion*).

DISCUSSION

Keratin 20 defines a subapical compartment containing Rab27b-associated FVs primed for apical insertion

Keratin 20 has an relatively narrow tissue distribution (Moll *et al.*, 1982) and is known to form a dense, subapical band in bladder and intestinal epithelia cells (Moll *et al.*, 1990, 1993; Veranic and Jezernik, 2002; Zhou *et al.*, 2003). FVs have been detected within this subapical band, and it has been suggested, based on the finding that stretching increases the hole size, that K20 might play a role in regulating vesicle delivery (Veranic and Jezernik, 2002; Kreft *et al.*, 2010). Our data demonstrate that the fusiform vesicles above and below the K20 band are associated with different sets of Rabs and their effectors (Figures 3, 4, 6, and 8) and that there is enhanced uroplakin accumulation in the subapical zone in areas with weaker K20 staining (Figure 8, A and B). Overall our results indicate that in mouse urothelial umbrella cells, the FVs undergo sequential changes in their associated

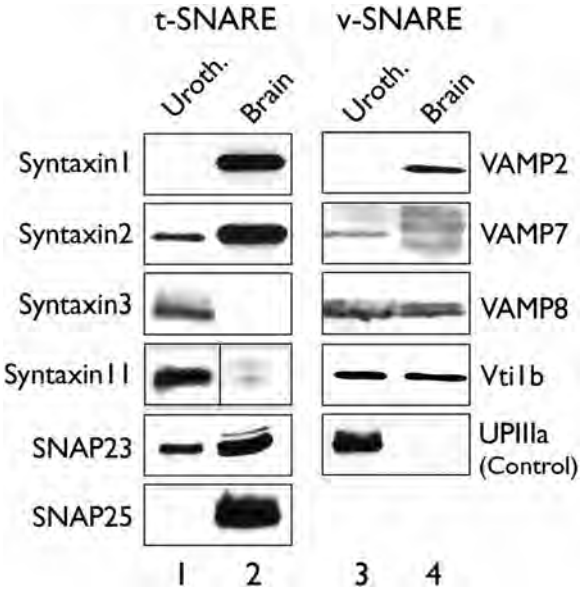

FIGURE 9: Mouse urothelial SNARE proteins. Total protein extracts of mouse urothelium (odd lanes) and brain (even lanes) immunoblotted using antibodies to t-SNAREs (left) and v-SNARES (right), as indicated. Anti-uroplakin IIIa was included as a control.

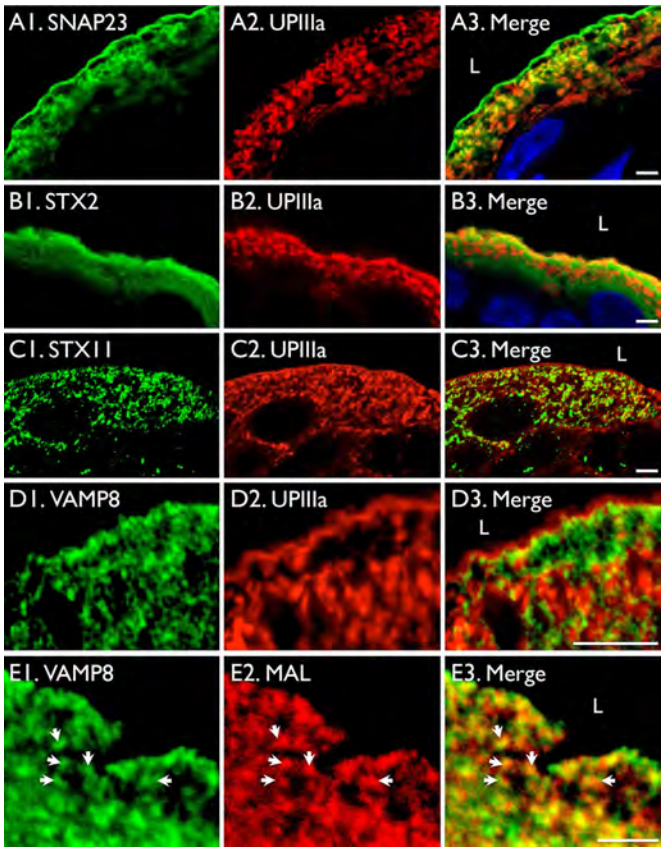

FIGURE 10: Immunolocalization of urothelial SNAREs. Normal mouse bladder sections were double-stained for confocal microscopy using antibodies to (A) SNAP23 (A1) and UPIIIa; (B) syntaxin 2 (B1) and UPIIIa (B2); (C) syntaxin 11 (C1) and UPIIIa (C2); (D) VAMP8 (D1) and UPIIIa (D2); and (E) VAMP8 (E1) and MAL (E2). Note that anti-SNAP23 and syntaxin 2 (STX2) stained apical membranes, anti-SNAP23 also labeled some cytoplasmic FVs, STX11and VAMP8 are mainly associated with cytoplasmic vesicles, and VAMP8 was on the periphery of FVs containing UPIIIa (D) and colocalized well with MAL (E; arrows), a marker of the hinge region (Zhou *et al.*, 2012). Bars, 5 µm.

trafficking molecules and that the K20 network forms a boundary between the subapical FVs that are primed for apical fusion and those of the cytoplasmic pool below. They further suggest that the K20 network might play a functional role in controlling the passage of FVs into the subapical compartment (see Figure 14 for a model of uroplakin exocytosis).

Rab27b plays a key role in regulating the trafficking and stability of the uroplakin-delivering vesicles

Even though we have not measured the apical insertion rate of uroplakin per se, our results strongly suggest that Rab27b plays a crucial role in uroplakin exocytosis. The importance of Rab27b, coupled with its binding protein, Slac2-a, is supported by the following data. First, Rab27b is associated with FVs near or at the apical membrane (Figures 1, 3, 4, 6, 8, and 12), and Rab27b knockout led to decreases in the uroplakin content and cellular height (related to cell volume) of the umbrella cells (Figure 7). Second, some of the Rab27b-containing FVs are associated with its effector proteins, Slac2-a and myosin Va (Figure 6). Mice with mutations in Slac2-a, which, together with myosin Va, is believed to be responsible for tethering secretory vesicles to and transport along the actin cytoskeletal network (Nagashima *et al.*, 2002; Westbroek *et al.*, 2004), have a similar umbrella cell phenotype to Rab27b-knockout mice, including decreased uroplakin content and cell height (Figure 7, C and D). Third, our studies revealed a tremendous accumulation of Slac2-a in the K20 zone (Figure 6, A–C), suggesting that either K20 per se or some of its associated proteins have a high affinity for Slac2-a. We hypothesize that the "tunnels" going through the K20 network must be bathed in a high concentration of Slac2-a, which may push the equilibrium in favor of replacing the FV-associated Rab11/8 by the Rab27b/Slac2-a complex. In other words, the tremendous increase in Slac2-a amounts past the lower K20 boundary may serve as a driving force for a switch of the FV-associated Rab from Rab11/8 to Rab27b/Slac2-a, thus facilitating apical targeting.

The importance of Rab27b, coupled with Slp2-a, in uroplakin trafficking is shown by our observations that Slp2-a 1) was highly expressed in umbrella cells and localized to subapical uroplakin vesicles and the apical membrane (Figure 8), 2) interacted with Rab27b (Figure 5C), and 3) almost completely disappeared in the Rab27b-null umbrella cells (Figures 5D and 8E). Similar destabilization of Slp2-a, which also interacts with Rab27a, was observed in Rab27a-defective T lymphocytes and in transfected Cos7 cells. This effect is attributed to its multiple PEST-like sequences, which are generally associated with rapid protein degradation (Holt *et al.*, 2008). These results strongly suggest that in urothelial umbrella cells, Rab27b interacts with and stabilizes Slp2-a and that the Rab27b/Slp2-a complex plays a key role in the apical delivery and docking of the uroplakin-delivering FVs.

The observed decrease in fusiform vesicles in the Rab27b-deficient umbrella cells (Figures 2 and 7) is likely the result of impaired exocytosis of uroplakin vesicles that are then shunted to a degradation pathway (Guo *et al.*, 2009; Vieira *et al.*, 2014) rather than to accelerated exocytosis followed by endocytic degradation. It is known, for example, that Rab27b knockout results in the inhibition of exocytosis as well as granule docking to the plasma membrane

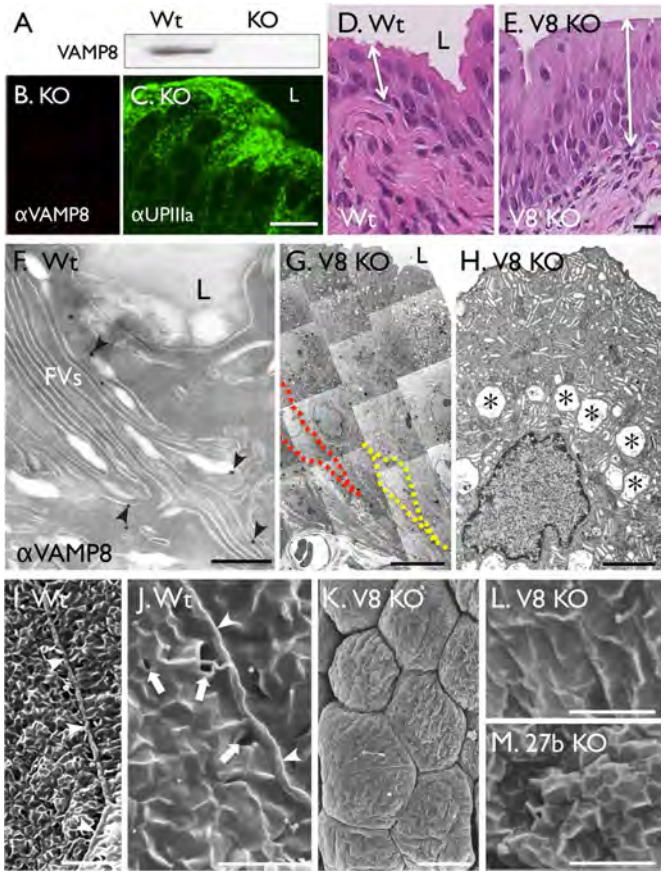

FIGURE 11: VAMP8 knockout blocked umbrella cell formation. (A, B) Immunoblotting and IF staining confirms the absence of VAMP8 protein in the knockout mouse urothelium. (C) UPIIIa-staining of the VAMP8-null urothelium, showing that the UP-stained superficial cells assumed an elongated, columnar morphology. Bar, 10 μm. (D, E) Hematoxylin and eosin–stained paraffin sections of (D) Wt and (E) VAMP8-null bladder, showing that the VAMP8-null urothelium was greatly thickened (double arrows) with columnar cells instead of the stratified squamous morphology in Wt urothelium. Bar, 10 μm. (F) EM localization of VAMP8 on ultrathin cryosections, showing significant labeling of the hinge areas (arrowheads). Bar, 0.25 μm. (G, H) Representative TEM images of the VAMP8-null urothelium, showing the columnar cells (G; a composite of 15 images; two lower columnar cells are outlined with dashed lines) with increased multivesicular bodies (H; asterisks). (I–M) Scanning EM of the bladder urothelial superficial cells of Wt mouse (I, J), VAMP8 KO (K, L), and Rab27b KO (M). Arrowheads in I and J denote the boundaries between neighboring cells (labeled 1–3). Note, in Wt (I, J), the apical plaques (0.6–0.8 μm) covering large cells (70–100 μm) and the occasional small "holes" (arrows in J; see *Discussion*); in K and L, the lack of apical plaques on the small VAMP8-null cells; and in M, the relatively normal apical surface with plaques in Rab27b-KO umbrella cells. Bars, 10 μm (G, I, K), 2 μm (H, J, L, and M).

in a wide range of secretory cells (reviewed in Fukuda, 2013). Similarly, in lacrimal gland cells, loss of Rab27b led to a decrease in subapical secretory vesicles and substantially more lysosomes and autophagosomes (Chiang *et al.*, 2011). Together these data suggest that the failure of uroplakin vesicles to tether onto the actin cytoskeleton in both the Rab27b-knockout and Slac2-a inactivation might destabilize them, leading to uroplakin degradation/depletion and eventually a decrease in cell volume and height (Figure 7D).

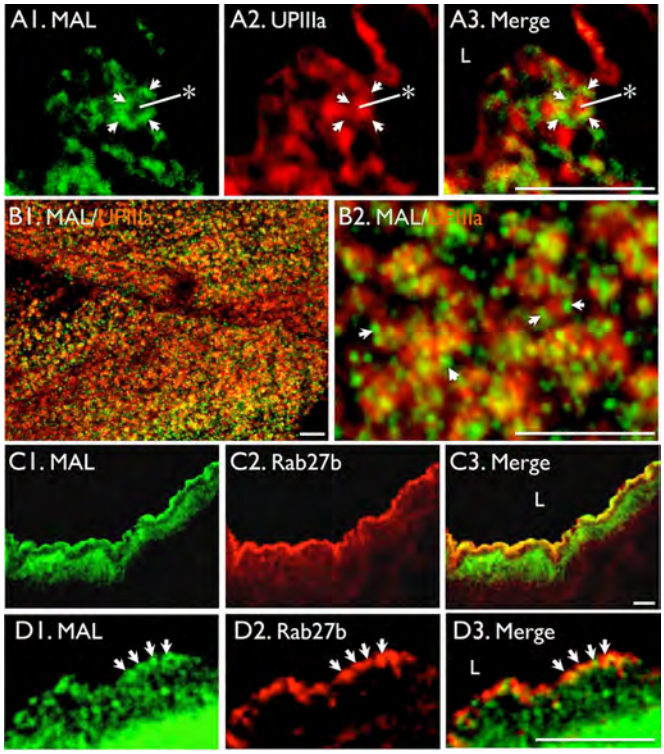

FIGURE 12: Immunolocalization of MAL in urothelial umbrella cells. Bladder paraffin sections or whole-mount urothelium (B) were immunostained for confocal microscopy using antibodies to (A) MAL (A1) and UPIIIa (A2), showing MAL localization (arrows) to the edge of a uroplakin vesicle (*). (B1, B) Staining of Mal and UPIIIa (B1), with a higher-magnification image (B2), confirming that Mal forms small dots (green; arrows), presumably in the hinges surrounding the (red) uroplakin plaques (Zhou *et al.*, 2012). (C, D) MAL (C1, D1) and Rab27b (C2, D2). Note, in C, the enrichment of MAL in the subapical zone above the K20 network, and in D, the colocalization of MAL with Rab27b (arrows) near the apical surface. Bars, 5 μm.

Rab11/8 and Rab27b function in the same pathway: a unifying concept

In our model of uroplakin exocytosis (Figure 14), Rab11 (stage Ia) and Rab8 (stage Ib) are depicted as mediators of the initial steps in uroplakin vesicle transport. This is based on the work of Khandelwal *et al.* (2008, 2013), who showed that Rab11a and subsequently Rab8a, together with myosin Vb, sequentially mediate the transport of FV from the TGN to, and their fusion with, the apical surface in response to stretch. Our localization data (Figures 3 and 4) support their conclusions. Khandelwal *et al.* (2013) also suggested that Rab27b regulates a separate, constitutive exocytic pathway. However, we found that Rab8a and Rab11a work upstream in the same pathway as Rab27b, based on the observations that 1) the Rab11/8-containing uroplakin vesicles are located farther away from the apical membrane than Rab27b (Figures 3 and 4) and 2) Rab8a and especially Rab11a partially colocalize with Rab27b in or near the K20 zone (Figures 3, B and D, and 4B). Note that Khandelwal *et al.* (2013) previously reported that, unlike our data showing Rab11 and Rab8 were primarily below the K20 zone, in rat umbrella cells Rab11 and Rab8 are mostly above the K20 meshwork (Khandelwal *et al.*, 2013). The species difference might account for this discrepancy between the two sets of data.

The sequential actions of Rab8a and Rab27b in umbrella cells might be analogous to those of Rab3 and Rab27a, which work in the same pathway in insulin-secreting pancreatic beta cells during

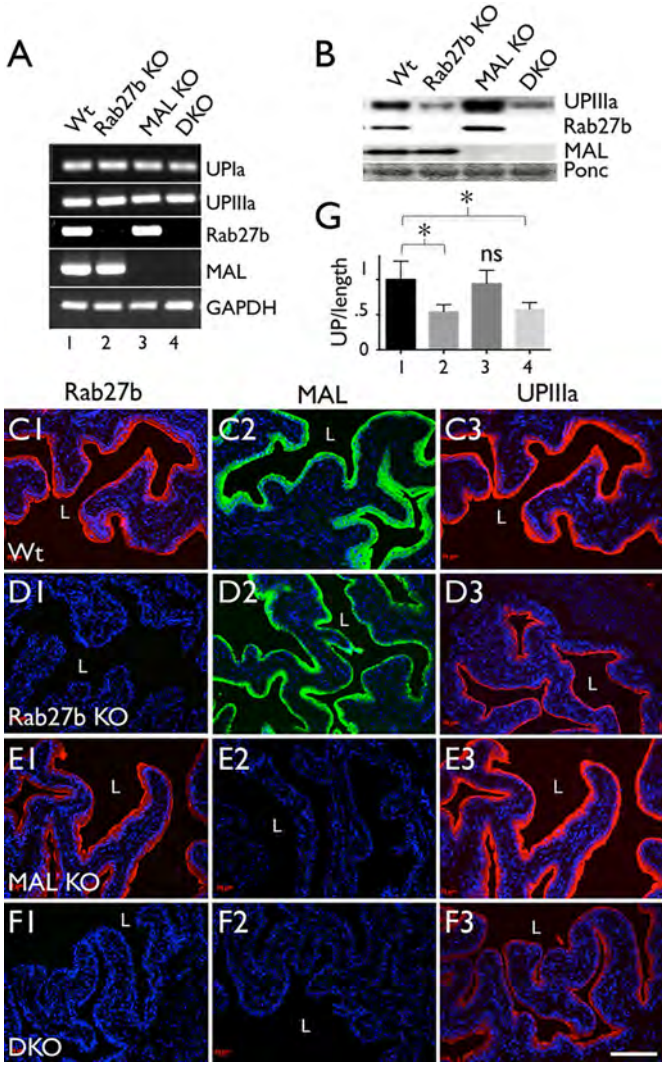

FIGURE 13: The urothelial phenotype of Rab27b-MAL double KO resembled that of Rab27b KO mice. (A) Detection by RT-PCR of the mRNAs encoding UPIa, UPIIIa, Rab27b, MAL, and GAPDH (loading control) in (lane 1) Wt, (lane 2) Rab27b-KO, (lane 3) MAL KO, and (lane 4) Rab27b-MAL double-KO (DKO) mouse urothelia. (B) Immunoblot detection of UPIIIa, Rab27b, and MAL in urothelial extracts from the same set of mice as in A. Ponc, Ponceau red staining of a common 40-kD band as a loading control. Note the absence of Rab27b, MAL, or both in the Rab27b KO, MAL KO, and double knockout, respectively. (C1–F3) Paraffin bladder sections from different mice (as indicated) were IF stained using antibodies to Rab27b (C1–F1), MAL (C2–F2), or UPIIIa (C3xF3). Some of the samples were serial sections (C1, C3, E1, E3), and all images for a given antibody had the same exposure time. Note that the UPIIIa level of the Rab27b-MAL DKO (F3) was comparable to that of the Rab27b-null urothelium (D3). (G) Quantification of UPIIIa staining intensity in umbrella cells (same method as in Figure 2C), showing a decrease in umbrella cell UPIIIa levels in the Rab27b-null (*$p < 0.025$) and DKO mice (*$p < 0.001$) as compared with Wt, whereas the UPIIIa intensity in the MAL-null sections did not differ significantly (ns, not significant with $p > 0.5$; number of analyzed images, from three independent experiments, are seven, three, six, and eight for the Wt, Rab27b KO, MAL KO, and double knockout, respectively; arbitrary units). Bar, 200 µm.

glucose stimulation but overlap in function (Cazares *et al.*, 2014). Whereas Rab27a controls the rapid exocytosis of insulin granules, Rab3 family members regulate the subsequent refilling of the releasable granule pools (Cazares *et al.*, 2014). However, inactivation of either Rab reduces but does not prevent insulin release, indicating that the two Rabs are to some extent functionally redundant, which might also be true of Rab27b and Rab8a in umbrella cells.

VAMP8 plays an indispensable role in uroplakin apical fusion

Our data indicate that SNARE proteins, particularly VAMP8, play a critical role in uroplakin trafficking. First, several SNAREs, including SNAP23, syntaxin 2, syntaxin 11, and VAMP8, are localized to uroplakin vesicles by confocal microscopy (Figure 10) and, for VAMP8, additionally by immuno-EM (Figure 11F). VAMP8 plays an important role in the regulated exocytosis of secretory granules at the apical plasma membrane of exocrine cells (Wang *et al.*, 2004, 2007; Messenger *et al.*, 2014). VAMP8 could play a similar role in umbrella cells controlling FV insertion into the apical membrane, which is a signal-mediated process regulated by bladder stretch (reviewed by Khandelwal *et al.*, 2009). Second, genetic ablation of the mouse VAMP8 gene led to a dramatic reduction of the diameter of the urothelial superficial cells, from 60–90 to 15–25 µm (Figure 11, B–K), and the absence of apical plaques (Figure 11L). These phenotypes are very similar to those found in uroplakin UPII- and UPIIIa-knockout mice (Hu *et al.*, 2000; Kong *et al.*, 2004). Knockout of either of these uroplakins prevents the formation of the 2D crystalline plaques, resulting in a failure of umbrella cell enlargement. These results suggest that VAMP8, along with its associated SNARE proteins and regulators, plays an indispensable role in the apical fusion of the uroplakin vesicles (stages IV and V in Figure 14) and that failure of this fusion to occur can potentially lead to the redirection of the FVs to undergo multivesicular body–mediated degradation. Note, however, that our data do not rule out the possibility that VAMP8 may perform additional functions, as it is also known to regulate endocytic vesicle fusion (Wong *et al.*, 1998; Antonin *et al.*, 2000).

Rab27b functions upstream of MAL: resolution of a controversy

Conflicting data exist regarding the function of MAL in apical membrane trafficking. Cheong *et al.* (1999) reported that MAL affects apical sorting at the level of the TGN, because MAL-depletion in MDCK cells impaired the apical transport of several apical proteins, including clusterin gp80, gp114, a glycophosphatidylinositol-linked protein, and influenza virus hemagglutinin (HA). Independently, Puertollano and Alonso (1999) also reported that MAL-depletion in MDCK cells reduced the raft association of HA. If it is assumed that raft association leads to apical targeting (see, however, Tall *et al.*, 2003), these data would suggest that MAL played a role in apical transport. However, our data are inconsistent with the suggested role of MAL in directing apical trafficking and instead support a role for MAL in facilitating apical fusion. First, we found that MAL depletion in MDCK cells had no effect on the apical transport of gp114, gp135, and (transfected) uroplakins, based on immunofluorescence staining (Zhou *et al.*, 2012). Second, in collaboration with Alonso's group, we confirmed another set of their data (Puertollano *et al.*, 1999) showing that MAL depletion reduces the rate by which membrane vesicles are inserted into the apical surface of MDCK cells (Zhou *et al.*, 2012). Third, we showed that genetic ablation of the mouse MAL gene led to FV accumulation in mouse urothelial umbrella cells. Conversely, MAL overexpression led to increased FV exocytosis accompanied by elevated endocytic degradation. These data strongly suggest that MAL facilitates, in both MDCK cells and in umbrella cells in vivo, the apical fusion of the uroplakin-delivery vesicles (Zhou *et al.*, 2012). Finally, and of most importance, our present data (Figure 13) indicate that double knockout of Rab27b and MAL genes caused a reduction of fusiform vesicle

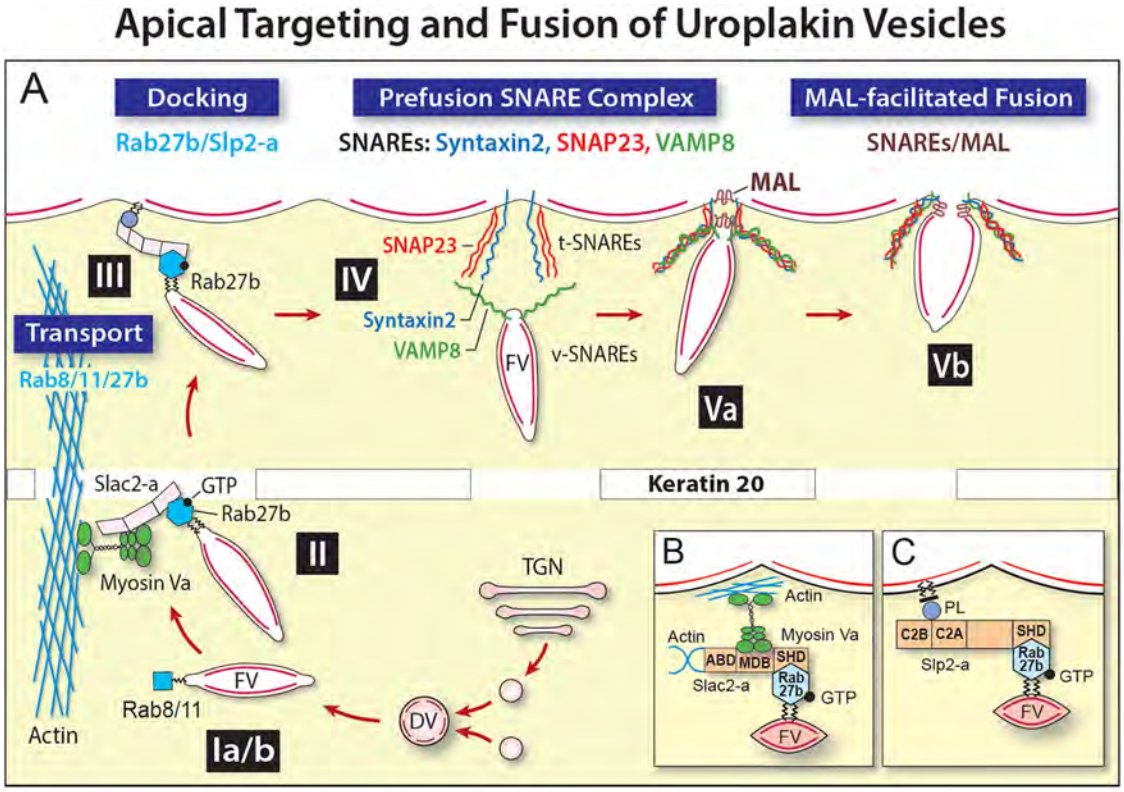

FIGURE 14: Model showing hypothetical steps by which the fusiform vesicles are transported to and fuse with the apical surface of urothelial umbrella cells. This model depicts a five-step process in which the uroplakin-delivering fusiform vesicles are transported via the sequential actions of Rab11, Rab8, and later Rab27 and their associated proteins, followed by membrane tethering and a final step of SNARE-mediated and MAL-facilitated fusion. The model is not drawn to scale. See the text for details.

number, that is, a phenotype similar to that seen in Rab27b-knockout mice (Figure 7, B and D; cf. Figure 2, A, B and D) but opposite to that of the MAL-knockout (FV accumulation; Zhou *et al.*, 2012). This result indicates that Rab27b functions upstream from MAL. Taken together, these data strongly support our suggestion that MAL functions mainly at the apical fusion step (Zhou *et al.*, 2012) rather than by directing apical transport at the TGN level (Figure 14).

Urothelial apical surface invaginations: the final step of FV insertion?

High-resolution scanning EM of the apical surface of normal mouse urothelium revealed for the first time the existence of many small "holes" that are actually deep invaginations with a maximal dimension roughly equal to that of the plaques (Figure 11J). These structures are scattered over the entire cell surface, with some concentration along the cell border (Figure 11, I and J). The fact that their linear diameter is similar to that of the plaque (0.6–0.9 μm) raises the interesting possibility that they represent the final stage of FV insertion into the apical surface (stage Vb, Figure 14). Note, however, that it is equally likely that they represent the initial stage of plaque internalization (Khandelwal *et al.*, 2010). Additional studies are needed to distinguish between these two possibilities.

The apical targeting and exocytosis of uroplakin vesicles are mediated via sequential and compartmentalized interactions with Rabs, SNAREs, and MAL: a unifying model

Taken together, our data suggest that Rab proteins and their effectors play sequential roles in the apical delivery of the uroplakin vesicles, which then fuse with the apical surface via a SNARE-mediated and MAL-facilitated process. On the basis of these data, we propose a hypothetical model with the following stages (Figure 14A):

Stage I. Rab11 and Rab8 function to transport FVs from the TGN to the K20 zone. This is based on the data of Khandelwal *et al.* (2008, 2013), as well as on our data showing that 1) Rab11a and Rab8a are localized primarily below the Rab27b-enriched subapical zone, and 2) in the transitional areas, they partially co-localize with Rab27b (Figures 3 and 4). These data suggest that Rab11 and Rab8 are involved in transporting the FVs from the TGN toward the K20-enriched zone, upstream of the Rab27b-mediated stages (Figure 14A).

Stage II. The Rab27b/Slac2/myosin Va complex mediates the tethering of uroplakin vesicles to cortical actin filaments (Figure 14, A and B). Coupled with the known functions of this complex in other cell types (Wu *et al.*, 2002), our data (Figures 6 and 7) suggest that in umbrella cells, this Rab27b complex enables the FVs to bind to, and be transported along, the actin filaments in order to reach the subapical compartment above the K20 zone.

Stage III. The Rab27b/Slp2-a complex mediates the docking of the FV to the apical membrane. We suggest that, above the K20 zone, this complex mediates docking of the FVs to the inner leaflet of the apical membrane (Figures 1E3, 8, and 14, A and C). This suggestion is consistent with data showing that Slp2-a binds to acidic phospholipids (Kuroda and Fukuda, 2004) and is

localized to the apical membrane of polarized epithelial cells (Galvez-Santisteban *et al.*, 2012).

Stage IV. There is formation of a prefusion SNARE complex. Our data suggest that VAMP8 and some other v-SNAREs and regulators are associated with the hinge region of the plaque (Figure 11F). Their binding to cognate partner t-SNAREs, for example, syntaxin 2 (Figure 10B1), on the apical hinges (Figure 10, A and B) would allow them to form a prefusion complex. Our data do not rule out the possibility that VAMP8, along with syntaxin 11 and SNAP23, which also localize to FVs (Figure 10, A and C), may also mediate FV homotypic fusion, as both syntaxins 2 and 11 have been shown to be in vitro partners of VAMP8 in other cell types (Fasshauer *et al.*, 1999; Ye *et al.*, 2012).

Stage V. There is MAL-facilitated, SNARE-mediated membrane fusion. Together with our earlier in vitro transfection and in vivo MAL-knockout and MAL-overexpression data (Zhou *et al.*, 2012), our present MAL-Rab27b double-knockout results (Figure 13) clearly establish that MAL acts downstream of Rab27b, most likely to facilitate the SNARE-mediated fusion of FVs with the apical membrane.

Rab27b, VAMP8, and MAL knockouts yield distinct umbrella cell phenotypes

An important finding of our work is that knockout of Rab27b, VAMP8, and MAL, which operate in the same UP delivery pathway (Figure 14), yielded distinct umbrella cell phenotypes. Most notably, the Rab27b-null and MAL-null urothelia have relatively large squamous umbrella cells (>50 µm), with an apical surface covered with plaques (Figure 11M), whereas the VAMP8-null urothelium has small columnar superficial cells (15–25 µm; Figure 11, D, E, G, and H) devoid of apical plaques (Figure 11L). These results can be explained by the following considerations. 1) Genetic ablation of Rab27b, which mediates two early steps of FV delivery (stages II and III, Figure 14), reduces the *efficiency* of apical UP delivery but allows the "leakage" of up to 30–40% of UPs (Figures 2D and 7D) to be apically delivered, possibly due to functional redundancies between Rab27b and Rab11/8 (or other Rabs; see earlier discussions on the functional redundancies between Rab27a and Rab3 in insulin delivery; Cazares *et al.*, 2014). This allows a sufficient amount of uroplakin plaques to reach the apical surface (Figure 11M) to sustain umbrella cell formation and enlargement (see later discussion). Thus Rab27b facilitates, but is not required for, the apical delivery of FVs (Figure 14). 2) Ablation of VAMP8, which is an integral component *required* for SNARE-mediated membrane fusion (stage Va, Figure 14), leads to the complete blockage of apical fusion of FVs, thus explaining the absence of apical plaques (Figure 11L) and the formation of small superficial cells (15–25 µm; Figure 11, K and L). 3) Ablation of MAL, which increases the *efficiency* of, but is not *required* for, the final step of SNARE-mediated fusion (stage Vb, Figure 14), leads to cytoplasmic accumulation of FVs (Zhou *et al.*, 2012). 4) Some of these proteins might have additional functions that can affect the phenotype. Overall our KO data revealed a high level of functional specialization in the individual protein components involved in UP exocytosis and provide in vivo functional data in support of our model (Figure 14). Moreover, the fact that VAMP8-null urothelium has small superficial cells, which are remarkably similar to those of the uroplakin knockouts, supports our earlier suggestion that adequate apical insertion of uroplakin plaques is required for the expansion and stabilization of the umbrella cell surface (Hu *et al.*, 2000; Kong *et al.*, 2004).

Unique features of fusiform vesicular exocytosis in urothelial umbrella cells

Taken together, our data suggest that the uroplakin-delivering FVs are transported toward, and fuse with, urothelial apical surface via the sequential action of several Rabs, SNAREs, and MAL (Figure 14). Whereas Rabs and SNAREs are involved in vesicle targeting and fusion in all cell types, the exocytic pathway of FVs has several unique features. First, unlike most other secretory vesicles that contain a flexible membrane and are mostly spherical in shape, FVs consist of two large, flat uroplakin plaques connected via a belt of flexible "hinge" membrane (Kachar *et al.*, 1999; Liang *et al.*, 1999; Hudoklin *et al.*, 2011). Although apical fusion of the FVs most likely occurs via the hinge area of both the FVs and the apical surface (Liang *et al.*, 1999), the size and rigidity of the plaques may require a facilitator, such as MAL, to lower the energy requirements for the SNARE-mediated membrane fusion. Note that our data do not rule out the possibility that MAL can function in membrane fusion per se. MAL is also expressed in many other cell types (Marazuela and Alonso, 2004), where it might have a related function. Second, in this system, keratin K20 defines a subapical compartment that contains a subpopulation of FVs equipped with appropriate trafficking molecules and are strategically located for apical fusion. A similar mechanism might operate in intestinal epithelial cells, in which K20 also forms a subapical band. Third, the exocytosis of FVs can be triggered by mechanical stretch (Lewis and de Moura, 1982; Truschel *et al.*, 1999; Yu *et al.*, 2009; Khandelwal *et al.*, 2013). In closing, an improved understanding of FV exocytosis, starting from the TGN all the way to apical fusion (Figure 14), provides a framework for future studies on urothelial membrane dynamics, which has major implications for the mechanism by which 1) urothelial surface area is reversibly adjusted during the normal micturition cycle or the excessive stretch induced by urinary tract obstruction, and 2) uropathogenic bacteria use uroplakin-trafficking pathways to facilitate their invasion into, and escape from, host urothelial cells.

MATERIALS AND METHODS

Mice

Wild-type C57BL/6J (Wt) mice were purchased from the Jackson Laboratory (Bar Harbor, ME). For all experiments, 4- to 6-wk-old Rab27b-null mice (Tolmachova *et al.*, 2007), MAL-null mice (Schaeren-Wiemers *et al.*, 2004), and Rab27b/MAL double-KO mice of the same C57BL/6J background were used. Rab27b/MAL double-KO mice were bred in our laboratory and showed no obvious defects in reproductive capacity or behavior. *Leaden* mice with a mutation in Slac2-a/melanophilin were from the Jackson Laboratory (C57Bl/6 J-In fz H54/+ +H54). VAMP8-null mice in a hybrid C57Bl/6-129/SVJ background were maintained as previously described (Wang *et al.*, 2004) and used at 8–12 wk of age. All animal protocols were in accordance with National Institutes of Health guidelines and were reviewed and approved by the Institutional Animal Care and Use Committees of New York University School of Medicine.

Reagents and antibodies

The primary antibodies used and their sources are listed in Supplemental Table S1. Alexa Fluor 488– and 594–conjugated secondary antibodies and ProLong Gold antifade reagent with 4′,6-diamidino-2-phenylindole were from Life Technologies (Grand Island, NY). Horseradish peroxidase (HRP)–conjugated secondary antibodies were from Jackson ImmunoResearch Laboratories (West Grove, PA).

Cell culture

Melan-A cells were cultured in DMEM (Life Technologies, Rockville, MD) supplemented with 10–15% fetal bovine serum (HyClone Laboratories, Logan, UT), penicillin (100 U/ml), and streptomycin (100 µg/ml) in a 5% CO_2 atmosphere as previously described (Zhou *et al.*, 2012). Ins-1 cells were maintained in RPMI1640 with 10 mM 4-(2-hydroxyethyl)-1-piperazineethanesulfonic acid (HEPES) and 10% fetal bovine serum as previously described (Kang *et al.*, 2005).

Immunofluorescence staining

The bladders of anesthetized mice were voided of urine by abdominal massage before they were excised and fixed in formaldehyde at 23 or 37°C (samples stained for Rab8 or actin) and either embedded in paraffin or processed for frozen sectioning (Guo *et al.*, 2009). Briefly, sections were incubated with primary antibodies at 4°C either for 1 h or overnight after deparaffinization and antigen retrieval for paraffin-embedded samples. Samples were subsequently incubated in secondary antibodies for 1 h and mounted in ProLong Gold. Images from the stained samples were obtained using an Axiophot microscope and camera or an LSM510 or LSM700 confocal microscope (Carl Zeiss, Thornwood, NY). Images were processed by enhancement of brightness and contrast only using ImageJ (National Institutes of Health, Bethesda, MD). To directly compare levels of UPIIIa and Rab27b in umbrella cells on stained sections, the original unenhanced images (obtained under identical exposure settings) were analyzed using ImageJ after identifying the keratin 8–labeled cell boundaries. Sample significance was determined using *t* tests (GraphPad Prism, La Jolla, CA). For the staining of whole-mount samples, mouse bladders were excised, cut in half, and pinned on a paraffin wax sheet before being fixed with 3.7% formaldehyde in phosphate-buffered saline (PBS) for 1 h. After washing and transfer to a 24-well dish, the samples were permeabilized for 1 h with 1% Triton X-100 in PBS before being stained for immunofluorescence as outlined.

RT-PCR

For RT-PCR analysis, total RNA was isolated from tissues or cultured cell lines using TRIzol Reagent (Life Technologies). cDNA was synthesized using SuperScript II or III reverse transcriptase (Life Technologies) according to the manufacturer's protocol.

Western blotting

A 20-µg amount of total protein was loaded and separated by SDS–PAGE (7.5, 10, or 12.5% polyacrylamide) and then transferred to nitrocellulose membrane (Hybond-ECL; Amersham Biosciences, Arlington Heights, IL). After Ponceau staining to confirm loading uniformity and blocking in 5% milk in PBS, membranes were incubated with primary antibodies at 4°C overnight before incubation with HRP-conjugated secondary antibodies. The specific protein bands were visualized using the Western Lightning Chemiluminescence Reagent Plus (PerkinElmer Life Sciences, Boston, MA).

Coimmunoprecipitation assays

For immunoprecipitation, total urothelial homogenates were incubated with 0.25% of Triton X-100 as described, and after centrifugation, supernatants (1 mg protein/ml) were incubated with anti-Slp2-a or anti-Slp4-a (10 µg/ml) for 1 h at 4°C before protein A–Sepharose beads were added (Amersham Biosciences) for another 1 h. After washing of the beads in the same buffer with 0.2% Triton X-100, proteins bound to the beads were eluted with SDS (1%) and separated by SDS–PAGE before Western blotting.

Electron microscopy

For conventional EM, freshly excised mouse bladders were cut into small pieces (<1 mm^3) and fixed with 2% glutaraldehyde in a 0.1 M cacodylate buffer (pH 7.4) and subsequently processed as previously described (Chen *et al.*, 2004). For immuno-EM, small pieces of freshly excised mouse bladders were fixed with 2% paraformaldehyde/0.2% glutaraldehyde in 0.1 M PHEM buffer (60 mM 1,4-piperazinediethanesulfonic acid, 25 mM HEPES, 10 mM ethylene glycol tetraacetic acid, 2 mM $MgCl_2$, pH 7.0) for 2 h at room temperature. Ultrathin frozen sections of the sucrose-embedded samples were produced and stained using gold secondary antibodies (Sigma-Aldrich, St. Louis, MO) as described previously (Guo *et al.*, 2009). Samples were incubated in primary antibody at 4°C overnight. The grids were viewed and images obtained using a JEM 200 CX microscope (JEOL USA, Peabody, MA).

For SEM, an abdominal incision was first made to allow access to the urinary bladder. Then PBS (120 µl/20 g) was injected into the bladder through a fine urethral catheter (Clay Adams Intramedic, inner diameter 0.28 mm; BD Scientific, Franklin Lakes, NJ). With the bladder walls under slight, constant stretch, 2% formaldehyde/2% glutaraldehyde in 0.1 M cacodylate buffer, pH 7.2, was pipetted over the bladder dropwise over a 5-min period, after which, the bladder was excised and bisected along the midline. Each half was submerged in fixative at 4°C for an additional 3 h before being transferred to 0.1 M cacodylate buffer (pH 7.2) and processed for SEM as previously described (Hudoklin *et al.*, 2012). Samples were dehydrated, critical point dried (CPD030; Bal-Tec, Balzers, Liechtenstein) and sputter coated with a thin layer of gold (10 nm) before image acquisition using a Quanta 250 SEM (FEI, Hillsboro, OR) operated at 10 kV (Andrade, 2015).

ACKNOWLEDGMENTS

We dedicate this article to Herbert Lepor to gratefully acknowledge his steadfast support of urological research at the New York University Langone Medical Center. We thank Melanie Pearson and Nicole Bornkamp for reading the manuscript and Robert Boyd for technical assistance. This work was supported by National Institutes of Health Grants DK-52206 (G.K., X.P.K., X.R.W., M.R., and T.-T.S.) and DK-39753 (T.-T.S.), the New York University Langone Medical Center Center of Excellence for Urological Diseases, the Goldstein Fund for Urological Research (X.R.W. and T.-T.S.), and Swiss National Science Foundation Grant 31003A-12510 (N.S.-W.). The New York University Langone Medical Center Microscopy Core is supported in part by NCRR RR023704 and RR024708 from the National Institutes of Health.

REFERENCES

Agola JO, Jim PA, Ward HH, Basuray S, Wandinger-Ness A (2011). Rab GTPases as regulators of endocytosis, targets of disease and therapeutic opportunities. Clin Genet 80, 305–318.

Andrade LR ((2015). Evidence for changes in beta- and gamma-actin proportions during inner ear hair cell life. Cytoskeleton (Hoboken) 72, 282–291.

Antonin W, Holroyd C, Tikkanen R, Honing S, Jahn R (2000). The R-SNARE endobrevin/VAMP-8 mediates homotypic fusion of early endosomes and late endosomes. Mol Biol Cell 11, 3289–3298.

Barral DC, Ramalho JS, Anders R, Hume AN, Knapton HJ, Tolmachova T, Collinson LM, Goulding D, Authi KS, Seabra MC (2002). Functional redundancy of Rab27 proteins and the pathogenesis of Griscelli syndrome. J Clin Invest 110, 247–257.

Born M, Pahner I, Ahnert-Hilger G, Jons T (2003). The maintenance of the permeability barrier of bladder facet cells requires a continuous fusion of discoid vesicles with the apical plasma membrane. Eur J Cell Biol 82, 343–350.

Cazares VA, Subramani A, Saldate JJ, Hoerauf W, Stuenkel EL (2014). Distinct actions of Rab3 and Rab27 GTPases on late stages of exocytosis of insulin. Traffic 15, 997–1015.
Chen Y, Guo X, Deng FM, Liang FX, Sun W, Ren M, Izumi T, Sabatini DD, Sun TT, Kreibich G (2003). Rab27b is associated with fusiform vesicles and may be involved in targeting uroplakins to urothelial apical membranes. Proc Natl Acad Sci USA 100, 14012–14017.
Chen X, Li C, Izumi T, Ernst SA, Andrews PC, Williams JA (2004). Rab27b localizes to zymogen granules and regulates pancreatic acinar exocytosis. Biochem Biophys Res Commun 323, 1157–1162.
Cheong KH, Zacchetti D, Schneeberger EE, Simons K (1999). VIP17/MAL, a lipid raft-associated protein, is involved in apical transport in MDCK cells. Proc Natl Acad Sci USA 96, 6241–6248.
Chiang L, Ngo J, Schechter JE, Karvar S, Tolmachova T, Seabra MC, Hume AN, Hamm-Alvarez SF (2011). Rab27b regulates exocytosis of secretory vesicles in acinar epithelial cells from the lacrimal gland. Am J Physiol Cell Physiol 301, C507–521.
Fasshauer D, Antonin W, Margittai M, Pabst S, Jahn R (1999). Mixed and non-cognate SNARE complexes. Characterization of assembly and biophysical properties. J Biol Chem 274, 15440–15446.
Fukuda M (2002). Synaptotagmin-like protein (Slp) homology domain 1 of Slac2-a/melanophilin is a critical determinant of GTP-dependent specific binding to Rab27A. J Biol Chem 277, 40118–40124.
Fukuda M (2006). Distinct Rab27A binding affinities of Slp2-a and Slac2-a/melanophilin: Hierarchy of Rab27A effectors. Biochem Biophys Res Commun 343, 666–674.
Fukuda M (2013). Rab27 effectors, pleiotropic regulators in secretory pathways. Traffic 14, 949–963.
Fukuda M, Kuroda TS (2002). Slac2-c (synaptotagmin-like protein homologue lacking C2 domains-c), a novel linker protein that interacts with Rab27, myosin Va/VIIa, and actin. J Biol Chem 277, 43096–43103.
Galvez-Santisteban M, Rodriguez-Fraticelli AE, Bryant DM, Vergarajauregui S, Yasuda T, Banon-Rodriguez I, Bernascone I, Datta A, Spivak N, Young K, *et al.* (2012). Synaptotagmin-like proteins control the formation of a single apical membrane domain in epithelial cells. Nat Cell Biol 14, 838–849.
Guo X, Tu L, Gumper I, Plesken H, Novak EK, Chintala S, Swank RT, Pastores G, Torres P, Izumi T, *et al.* (2009). Involvement of vps33a in the fusion of uroplakin-degrading multivesicular bodies with lysosomes. Traffic 10, 1350–1361.
Holt O, Kanno E, Bossi G, Booth S, Daniele T, Santoro A, Arico M, Saegusa C, Fukuda M, Griffiths GM (2008). Slp1 and Slp2-a localize to the plasma membrane of CTL and contribute to secretion from the immunological synapse. Traffic 9, 446–457.
Hu CC, Bachmann T, Zhou G, Liang FX, Ghiso J, Kreibich G, Sun TT (2008). Assembly of a membrane receptor complex: roles of the uroplakin II prosequence in regulating uroplakin bacterial receptor oligomerization. Biochem J 414, 195–203.
Hu CC, Liang FX, Zhou G, Tu L, Tang CH, Zhou J, Kreibich G, Sun TT (2005). Assembly of urothelial plaques: tetraspanin function in membrane protein trafficking. Mol Biol Cell 16, 3937–3950.
Hu P, Deng FM, Liang FX, Hu CM, Auerbach AB, Shapiro E, Wu XR, Kachar B, Sun TT (2000). Ablation of uroplakin III gene results in small urothelial plaques, urothelial leakage, and vesicoureteral reflux. J Cell Biol 151, 961–972.
Hu P, Meyers S, Liang FX, Deng FM, Kachar B, Zeidel ML, Sun TT (2002). Role of membrane proteins in permeability barrier function: uroplakin ablation elevates urothelial permeability. Am J Physiol Renal Physiol 283, F1200–F1207.
Hudoklin S, Jezernik K, Neumuller J, Pavelka M, Romih R (2011). Urothelial plaque formation in post-Golgi compartments. PLoS One 6, e23636.
Hudoklin S, Jezernik K, Neumuller J, Pavelka M, Romih R (2012). Electron tomography of fusiform vesicles and their organization in urothelial cells. PLoS One 7, e32935.
Hutagalung AH, Novick PJ (2011). Role of Rab GTPases in membrane traffic and cell physiology. Physiol Rev 91, 119–149.
Jahn R, Scheller RH (2006). SNAREs—engines for membrane fusion. Nat Rev Mol Cell Biol 7, 631–643.
Kachar B, Liang F, Lins U, Ding M, Wu XR, Stoffler D, Aebi U, Sun TT (1999). Three-dimensional analysis of the 16 nm urothelial plaque particle: luminal surface exposure, preferential head-to-head interaction, and hinge formation. J Mol Biol 285, 595–608.
Kang G, Chepurny OG, Rindler MJ, Collis L, Chepurny Z, Li WH, Harbeck M, Roe MW, Holz GG (2005). A cAMP and Ca2+ coincidence detector in support of Ca2+-induced Ca2 +release in mouse pancreatic beta cells. J Physiol 566, 173–188.
Khandelwal P, Abraham SN, Apodaca G (2009). Cell biology and physiology of the uroepithelium. Am J Physiol Renal Physiol 297, F1477–1501.
Khandelwal P, Prakasam HS, Clayton DR, Ruiz WG, Gallo LI, van Roekel D, Lukianov S, Peranen J, Goldenring JR, Apodaca G (2013). A Rab11a-Rab8a-Myo5B network promotes stretch-regulated exocytosis in bladder umbrella cells. Mol Biol Cell 24, 1007–1019.
Khandelwal P, Ruiz WG, Apodaca G (2010). Compensatory endocytosis in bladder umbrella cells occurs through an integrin-regulated and RhoA- and dynamin-dependent pathway. EMBO J 29, 1961–1975.
Khandelwal P, Ruiz WG, Balestreire-Hawryluk E, Weisz OA, Goldenring JR, Apodaca G (2008). Rab11a-dependent exocytosis of discoidal/fusiform vesicles in bladder umbrella cells. Proc Natl Acad Sci USA 105, 15773–15778.
Kong XT, Deng FM, Hu P, Liang FX, Zhou G, Auerbach AB, Genieser N, Nelson PK, Robbins ES, Shapiro E, *et al.* (2004). Roles of uroplakins in plaque formation, umbrella cell enlargement, and urinary tract diseases. J Cell Biol 167, 1195–1204.
Kreft ME, Hudoklin S, Jezernik K, Romih R (2010). Formation and maintenance of blood-urine barrier in urothelium. Protoplasma 246, 3–14.
Kuroda TS, Fukuda M (2004). Rab27A-binding protein Slp2-a is required for peripheral melanosome distribution and elongated cell shape in melanocytes. Nat Cell Biol 6, 1195–1203.
Lewis SA, de Moura JL (1982). Incorporation of cytoplasmic vesicles into apical membrane of mammalian urinary bladder epithelium. Nature 297, 685–688.
Liang F, Kachar B, Ding M, Zhai Z, Wu XR, Sun TT (1999). Urothelial hinge as a highly specialized membrane: detergent-insolubility, urohingin association, and in vitro formation. Differentiation 65, 59–69.
Lin JH, Wu XR, Kreibich G, Sun TT (1994). Precursor sequence, processing, and urothelium-specific expression of a major 15-kDa protein subunit of asymmetric unit membrane. J Biol Chem 269, 1775–1784.
Liu Y, Memet S, Saban R, Kong X, Aprikian P, Sokurenko E, Sun TT, Wu XR (2015). Dual ligand/receptor interactions activate urothelial defenses against uropathogenic E. coli. Sci Rep 5, 16234.
Marazuela M, Alonso MA (2004). Expression of MAL and MAL2, two elements of the protein machinery for raft-mediated transport, in normal and neoplastic human tissue. Histol Histopathol 19, 925–933.
Messenger SW, Falkowski MA, Thomas DD, Jones EK, Hong W, Gaisano HY, Boulis NM, Groblewski GE (2014). Vesicle associated membrane protein 8 (VAMP8)-mediated zymogen granule exocytosis is dependent on endosomal trafficking via the constitutive-like secretory pathway. J Biol Chem 289, 28040–28053.
Min G, Wang H, Sun TT, Kong XP (2006). Structural basis for tetraspanin functions as revealed by the cryo-EM structure of uroplakin complexes at 6-A resolution. J Cell Biol 173, 975–983.
Min G, Zhou G, Schapira M, Sun TT, Kong XP (2003). Structural basis of urothelial permeability barrier function as revealed by cryo-EM studies of the 16 nm uroplakin particle. J Cell Sci 116, 4087–4094.
Moll R, Franke WW, Schiller DL, Geiger B, Krepler R (1982). The catalog of human cytokeratins: patterns of expression in normal epithelia, tumors and cultured cells. Cell 31, 11–24.
Moll R, Schiller DL, Franke WW (1990). Identification of protein IT of the intestinal cytoskeleton as a novel type I cytokeratin with unusual properties and expression patterns. J Cell Biol 111, 567–580.
Moll R, Zimbelmann R, Goldschmidt MD, Keith M, Laufer J, Kasper M, Koch PJ, Franke WW (1993). The human gene encoding cytokeratin 20 and its expression during fetal development and in gastrointestinal carcinomas. Differentiation 53, 75–93.
Nagashima K, Torii S, Yi Z, Igarashi M, Okamoto K, Takeuchi T, Izumi T (2002). Melanophilin directly links Rab27a and myosin Va through its distinct coiled-coil regions. FEBS Lett 517, 233–238.
Puertollano R, Alonso MA (1999). MAL, an integral element of the apical sorting machinery, is an itinerant protein that cycles between the trans-Golgi network and the plasma membrane. Mol Biol Cell 10, 3435–3447.
Puertollano R, Martin-Belmonte F, Millan J, de Marco MC, Albar JP, Kremer L, Alonso MA (1999). The MAL proteolipid is necessary for normal apical transport and accurate sorting of the influenza virus hemagglutinin in Madin-Darby canine kidney cells. J Cell Biol 145, 141–151.
Roland JT, Lapierre LA, Goldenring JR (2009). Alternative splicing in class V myosins determines association with Rab10. J Biol Chem 284, 1213–1223.
Romih R, Veranic P, Jezernik K (1999). Actin filaments during terminal differentiation of urothelial cells in the rat urinary bladder. Histochem Cell Biol 112, 375–380.
Schaeren-Wiemers N, Bonnet A, Erb M, Erne B, Bartsch U, Kern F, Mantei N, Sherman D, Suter U (2004). The raft-associated protein MAL is

required for maintenance of proper axon–glia interactions in the central nervous system. J Cell Biol 166, 731–742.
Sun T-T, Kreibich G, Pellicer A, Kong XP, Wu XR ((2013). Uroplakins as a unique tetraspanin network. In: Tetraspanins, ed. F Berditchevski and E Rubinstein, Dordrecht, Netherlands: Springer, 299–320.
Sun Y, Chiu TT, Foley KP, Bilan PJ, Klip A (2014). Myosin Va mediates Rab8A-regulated GLUT4 vesicle exocytosis in insulin-stimulated muscle cells. Mol Biol Cell 25, 1159–1170.
Tall RD, Alonso MA, Roth MG (2003). Features of influenza HA required for apical sorting differ from those required for association with DRMs or MAL. Traffic 4, 838–849.
Tolmachova T, Abrink M, Futter CE, Authi KS, Seabra MC (2007). Rab27b regulates number and secretion of platelet dense granules. Proc Natl Acad Sci USA 104, 5872–5877.
Truschel ST, Ruiz WG, Shulman T, Pilewski J, Sun TT, Zeidel ML, Apodaca G (1999). Primary uroepithelial cultures. A model system to analyze umbrella cell barrier function. J Biol Chem 274, 15020–15029.
Truschel ST, Wang E, Ruiz WG, Leung SM, Rojas R, Lavelle J, Zeidel M, Stoffer D, Apodaca G (2002). Stretch-regulated exocytosis/endocytosis in bladder umbrella cells. Mol Biol Cell 13, 830–846.
Tu L, Sun TT, Kreibich G (2002). Specific heterodimer formation is a prerequisite for uroplakins to exit from the endoplasmic reticulum. Mol Biol Cell 13, 4221–4230.
Veranic P, Jezernik K (2002). Trajectorial organisation of cytokeratins within the subapical region of umbrella cells. Cell Motil Cytoskeleton 53, 317–325.
Vieira N, Deng FM, Liang FX, Liao Y, Chang J, Zhou G, Zheng W, Simon JP, Ding M, Wu XR, *et al.* (2014). SNX31: a novel sorting nexin associated with the uroplakin-degrading multivesicular bodies in terminally differentiated urothelial cells. PLoS One 9, e99644.
Walz T, Haner M, Wu XR, Henn C, Engel A, Sun TT, Aebi U (1995). Towards the molecular architecture of the asymmetric unit membrane of the mammalian urinary bladder epithelium: a closed "twisted ribbon" structure. J Mol Biol 248, 887–900.
Wang EC, Lee JM, Ruiz WG, Balestreire EM, von Bodungen M, Barrick S, Cockayne DA, Birder LA, Apodaca G (2005). ATP and purinergic receptor-dependent membrane traffic in bladder umbrella cells. J Clin Invest 115, 2412–2422.
Wang CC, Ng CP, Lu L, Atlashkin V, Zhang W, Seet LF, Hong W (2004). A role of VAMP8/endobrevin in regulated exocytosis of pancreatic acinar cells. Dev Cell 7, 359–371.
Wang CC, Shi H, Guo K, Ng CP, Li J, Gan BQ, Chien Liew H, Leinonen J, Rajaniemi H, Zhou ZH, *et al.* (2007). VAMP8/endobrevin as a general vesicular SNARE for regulated exocytosis of the exocrine system. Mol Biol Cell 18, 1056–1063.
Westbroek W, Lambert J, De Schepper S, Kleta R, Van Den Bossche K, Seabra MC, Huizing M, Mommaas M, Naeyaert JM (2004). Rab27b is up-regulated in human Griscelli syndrome type II melanocytes and linked to the actin cytoskeleton via exon F-Myosin Va transcripts. Pigment Cell Res 17, 498–505.
Wong SH, Zhang T, Xu Y, Subramaniam VN, Griffiths G, Hong W (1998). Endobrevin, a novel synaptobrevin/VAMP-like protein preferentially associated with the early endosome. Mol Biol Cell 9, 1549–1563.
Wu XR, Kong XP, Pellicer A, Kreibich G, Sun TT (2009). Uroplakins in urothelial biology, function, and disease. Kidney Int 75, 1153–1165.
Wu XR, Lin JH, Walz T, Haner M, Yu J, Aebi U, Sun TT (1994). Mammalian uroplakins. A group of highly conserved urothelial differentiation-related membrane proteins. J Biol Chem 269, 13716–13724.
Wu XR, Manabe M, Yu J, Sun TT (1990). Large scale purification and immunolocalization of bovine uroplakins I, II, and III. Molecular markers of urothelial differentiation. J Biol Chem 265, 19170–19179.
Wu XR, Sun TT (1993). Molecular cloning of a 47 kDa tissue-specific and differentiation-dependent urothelial cell surface glycoprotein. J Cell Sci 106, 31–43.
Wu XR, Sun T-T, Medina JJ (1996). In vitro binding of type 1-fimbriated Escherichia coli to uroplakins Ia and Ib: relation to urinary tract infections. Proc Natl Acad Sci USA 93, 9630–9635.
Wu XS, Rao K, Zhang H, Wang F, Sellers JR, Matesic LE, Copeland NG, Jenkins NA, Hammer JA 3rd (2002). Identification of an organelle receptor for myosin-Va. Nat Cell Biol 4, 271–278.
Ye S, Karim ZA, Al Hawas R, Pessin JE, Filipovich AH, Whiteheart SW (2012). Syntaxin-11, but not syntaxin-2 or syntaxin-4, is required for platelet secretion. Blood 120, 2484–2492.
Yu J, Lin JH, Wu XR, Sun TT (1994). Uroplakins Ia and Ib, two major differentiation products of bladder epithelium, belong to a family of four transmembrane domain (4TM) proteins. J Cell Biol 125, 171–182.
Yu J, Manabe M, Wu XR, Xu C, Surya B, Sun TT (1990). Uroplakin I: a 27-kD protein associated with the asymmetric unit membrane of mammalian urothelium. J Cell Biol 111, 1207–1216.
Yu W, Khandelwal P, Apodaca G (2009). Distinct apical and basolateral membrane requirements for stretch-induced membrane traffic at the apical surface of bladder umbrella cells. Mol Biol Cell 20, 282–295.
Zhou G, Liang FX, Romih R, Wang Z, Liao Y, Ghiso J, Luque-Garcia JL, Neubert TA, Kreibich G, Alonso MA, *et al.* (2012). MAL facilitates the incorporation of exocytic uroplakin-delivering vesicles into the apical membrane of urothelial umbrella cells. Mol Biol Cell 23, 1354–1366.
Zhou G, Mo WJ, Sebbel P, Min G, Neubert TA, Glockshuber R, Wu XR, Sun TT, Kong XP (2001). Uroplakin Ia is the urothelial receptor for uropathogenic Escherichia coli: evidence from in vitro FimH binding. J Cell Sci 114, 4095–4103.
Zhou Q, Toivola DM, Feng N, Greenberg HB, Franke WW, Omary MB (2003). Keratin 20 helps maintain intermediate filament organization in intestinal epithelia. Mol Biol Cell 14, 2959–2971.

Supplemental Materials

Molecular Biology of the Cell

Wankel et al.

Supplemental Table. Sources and properties of the antibodies used in this study.

Supplemental Table 1

Antigen	Species (Ab)	Source	Catolog #	WB Dilu	IFM Dilu
Actin	Mouse	DSHB[1]	JLA20	1/500	1/50
K8	Rat	DSHB[2]	Troma-1	1/500	1/25
K20	Mouse	Abcam	Ab854	-	1/50
Mal	Goat	Santa Cruz	SC-46171	1/100	1/50
MyoVa	Rabbit	Sigma Aldrich	M4812	1/500	1/100
Rab8	Mouse	BD Biosci	610844	1/500	1/50
Rab11	Mouse	BD Biosci	610657	1/1000	1/100
Rab27b	Goat	Lifespan	B12412	1/500	1/100
Rab27b	Rabbit	Proteintech	13412-1	1/500	1/250
Slac2a	Rabbit	Fukuda Lab[3]	-	1/500	1/100
Slac2a	Rabbit	Proteinech	10338-1	1/500	1/100
Slp1	Rabbit	Fukuda Lab[4]	-	1/500	1/100
Slp2a	Rabbit	Fukuda Lab[4]	-	1/1000	1/100
Slp4a	Rabbit	Fukuda Lab[5]	-	1/500	1/100
Slp5	Rabbit	Fukuda Lab[6]	-	1/500	1/100
SNAP23	Rabbit	SySy	111202	1/1000	1/100
STX1	Mouse	SySy	110011	1/1000	1/1000
STX2	Rabbit	SySy	110022	1/1000	1/100
STX3	Rabbit	Abcam	Ab4113	1/1000	1/50
STX11	Rabbit	SySy	110113	1/1000	1/100
UPIIIa (AU1)	Mouse	Sun Lab[7]	-	1/3000	1/250
UPIIIa/AUM	Rabbit	Sun Lab[8]	-	1/3000	1/250
VAMP2	Rabbit	SySy	104211	1/10000	1/500
VAMP8	Rabbit	SySy	104302	1/1000	1/100
Vti1b	Mouse	BD Biosci	611404	1/500	1/50

Abbreviations: WB (Western Blot), IFM (Immunofluorescence Microscopy)

References:

1. Lin, J.J.-C. (1981) Proc Nat'l Acad Sci., 78:2335
2. Brûlet, P. (1980) Proc Nat'l Acad Sci., 77:4113
3. Fukuda, M. (2002) J Biol Chem., 277:40118
4. Kuroda, T. (2002) J Biol Chem., 277: 9212
5. Fukuda, M. (2002) J Biol Chem., 277: 39673
6. Kuroda, T. (2002) J Biol Chem., 293: 899
7. Liang, F. (2001) Biochem J., 355:13
8. Wu, XR. (1993) J Cell Sci., 106:31